UNIVERSIDADE FEDERAL DE MINAS GERAIS

PROGRAMA DE PÓS-GRADUAÇÃO EM

ENGENHARIA MECÂNICA

EXPERIMENTAL AND THEORETICAL STUDY OF THE DYNAMIC RESPONSE OF A SMALL SIZE CO_2 DIRECT EXPANSION SOLAR ASSISTED HEAT PUMP

TIAGO DE FREITAS PAULINO

Belo Horizonte, February 22nd, 2019

Tiago de Freitas Paulino

EXPERIMENTAL AND THEORETICAL STUDY OF THE DYNAMIC RESPONSE OF A SMALL SIZE CO_2 DIRECT EXPANSION SOLAR ASSISTED HEAT PUMP

Submitted in partial fulfillment of the requirements for the degree of Doctorate in Mechanical Engineering in the Graduate Program of Mechanical Engineering at Universidade Federal de Minas Gerais.
Field: Energy and Sustainability
Advisor: Prof. Antônio Augusto Torres Maia
Co-advisor: Prof. Luiz Machado

Belo Horizonte
Engineering School of UFMG
2019

Paulino, Tiago de Freitas.
P328e Experimental and theoretical study of the dynamic response of a small size CO2 direct expasion solar assisted heat pump [manuscrito] / Tiago de Freitas Paulino. – 2019.
76 f., enc.: il.

Orientador: Antônio Augusto Torres Maia.
Coorientador: Luiz Machado.

Tese (doutorado) - Universidade Federal de Minas Gerais, Escola de Engenharia.

Apêndices: f. 67-76.

Bibliografia: f. 61-66.

1. Engenharia mecânica - Teses. 2. Dióxido de carbono - Teses. 3. Energia solar - Teses. 3. Bombas de calor - Teses. I. Maia, Antônio Augusto Torres. II. Machado, Luiz. III. Universidade Federal de Minas Gerais. Escola de Engenharia. IV. Título.

CDU: 621(043)

UNIVERSIDADE FEDERAL DE MINAS GERAIS
PROGRAMA DE PÓS-GRADUAÇÃO EM ENGENHARIA MECÂNICA
Av. Antônio Carlos, 6627 - Campus Universitário
31270-901 – Belo Horizonte – MG
Tel.:+55 31 3409.5145
E-mail: cpgmec@demec.ufmg.br

"EXPERIMENTAL AND THEORETICAL STUDY OF THE DYNAMIC RESPONSE OF A SMALL SIZE CO2 DIRECT EXPANSION SOLAR ASSISTED HEAT PUMP"

TIAGO DE FREITAS PAULINO

Tese submetida à Banca Examinadora designada pelo Colegiado do Programa de Pós-Graduação em Engenharia Mecânica da Universidade Federal de Minas Gerais, como parte dos requisitos necessários à obtenção do título de **"Doutor em Engenharia Mecânica"**, na área de concentração de **"Energia e Sustentabilidade".**

Tese aprovada no dia 22 de fevereiro de 2019.

Por:

Prof. Antônio Augusto Torres Maia
Orientador - Departamento de Engenharia Mecânica/ UFMG

Prof. Luiz Machado
Co-orientador - Departamento de Engenharia Mecânica/ UFMG

Prof. Raphael Nunes de Oliveira
Departamento de Engenharia Mecânica/ UFMG

Prof. Rudolf Huebner
Departamento de Engenharia Mecânica/ UFMG

Prof. Willian Moreira Duarte
Centro Universitário de Belo Horizonte

Prof. Paulo Eduardo Lopes Barbieri
Centro Federal de Educação Tecnológica de Minas Gerais

DEDICATION

I dedicate this work to my wife Eliene, to my children Artur and Helena and to my parents Vicente and Odaci.

ACKNOWLEDGMENTS

I chose to write this section of the thesis at last. This section symbolizes the end of this journey, and it is a way to say thank you to those who supported me during this period.

First of all, I have to thank God for supporting me with his grace and the Virgin Mary for her protection.

I would like to thank my family for encouraging me at this stage in my career: my wife Eliene for the patience, affection, prayers and for walking with me; my children Artur and Helena, you always put a smile on my face; my parents Vicente and Odaci, you teach me new things every day; my sister Aninha; and Edite, Antônio, Eliete, Giliarde and Felipe, my new family. You have my gratitude and love.

I want to thank my supervisor Professor Antônio Augusto Torres Maia and my co-supervisor Professor Luiz Machado for their continuous guidance, inspirations and encouragement. Professors Bjorn Palm and Samer Sawalha for hosting me at KTH and for the guidance durant this part of my Ph.D. Professor Raphael Oliveira for useful insight and assistance.

I want to express thanks to Professor Ricardo Koury (was my supervisor in this Ph.D. thesis and unfortunately, we missed him), who provided insight and expertise that greatly assisted this thesis.

I want to thank all Professors of Mechanical graduate program. I want to thank everyone that works in the secretary of Mechanical graduate program at UFMG. I want to thank Mr. Edson who supported me so much.

I want to thank my colleagues from GREA: Willian, Sabrina, Fernando, Juan, Leonardo, Túlio, Ivana, Cleisson, Cássio, Hélio, Rodrigo, Pietro, Pedro Ivo and Ramon. I also want to thank my colleagues from KTH: Tianhao, Luis, Enrique, Amir, David, Bezahd and Mazyar.

I want to thank CEFET-MG for providing conditions so that I could developed this thesis. In especially, my colleagues Leandro Cristino, André Ferreira and André Oliveira.

I want to thank all my family and friends. In specially, Everthon and Breno that give me important help in some moments.

Finally, I want to thank Fundação de Amparo à Pesquisa do Estado de Minas Gerais (FAPEMIG). This work was supported by FAPEMIG, through the project FAPEMIG AUC-00032-16.

ABSTRACT

Providing adequate and low-cost control is an important step in the use of direct expansion solar assisted heat pump (DX-SAHP) in replacement of the electric showers in the Brazilian residences. In that way, design a low-cost controller to regulate the hot water temperature in 60°C (to storage) and 45°C (to direct consumption) is the first goal of this study. Experimental tests demonstrated the capacity of the control system to keep hot water in the correct temperature in different environment and system conditions. The second goal of this study is to evaluate the expansion valve opening. The impact of a fixed aperture in the functioning and on the performance of these systems is not well known, especially for small-size systems. In this context, it is presented an experimental analysis of the influence of the expansion valve opening on the performance of a carbon dioxide (CO_2) DX-SAHP. Experimental tests were carried out considering solar radiations about 48 W/m² and 715 W/m² in which the coefficient of performance (COP) observed were 2.21 and 2.58, respectively. The value of the expansion device opening that leads to the maximum COP was similar, regardless the solar radiation. In consequence, for a small CO_2 DX-SAHP, using a basic cycle configuration (where the expansion device is used to control the optimum high pressure and consequently the COP), a low-cost embedded system water temperature control and a static expansion device would be suitable for proper control. Finally, the third goal of this study is to evaluate the effects of the sudden variations in the solar radiation on the superheat. The mathematical model was validated using experimental data and employed to perform several simulations. The results obtained with the mathematical model revealed that a small variation of the solar radiation leads to a significant variation in the superheat, therefore requiring an immediate action of the expansion device. In conclusion, an electronic expansion valve would be better suited to meet the needs of rapid interventions on the mass flow rate at the evaporator inlet and also the DX-SAHP could operate in a continuous transient condition in some seasons.

KeyWords: Heat pump, Solar assisted, CO_2, Dynamic response, Direct expansion.

RESUMO

Prover controle adequado e de baixo custo é uma importante etapa no processo de uso da bomba de calor de expansão direta assistida por energia solar (DX-SAHP) em substituição aos chuveiros elétricos nas residências brasileiras. Neste sentido, projetar um controlador de baixo custo para regular a temperatura de água quente em 60°C (armazenamento) e 45°C (consumo direto) é o primeiro objetivo deste trabalho. Testes experimentais mostraram a capacidade do controlador em manter, em diferentes condições ambientais e de operação, a temperatura da água quente no valor desejado. O segundo objetivo deste estudo é avaliar a área de abertura do dispositivo de expansão. Os efeitos da manutenção de uma abertura fixa para o dispositivo de expansão no funcionamento e no desempenho do sistema, sobretudo os de pequeno porte, não são bem conhecidos. Neste contexto, é realizada uma análise experimental da influência da abertura do dispositivo de expansão no desempenho de uma CO_2 DX-SAHP. Experimentos foram realizados com radiações próximas a 48 W/m² e 715 W/m², resultando em coeficiente de performance (COP) iguais a 2,21 e 2,58 respectivamente. Observou-se que a abertura do dispositivo de expansão para a qual obteve-se o COP máximo foi similar independente da radiação solar. Em consequência, para uma CO_2 DX-SAHP de pequeno porte, operando em uma configuração de ciclo básico (na qual o dispositivo de expansão é utilizado para controlar a pressão de alta ótima e consequentemente o COP), um sistema embarcado de baixo custo para controle da temperatura de água e um dispositivo de expansão estático podem proporcionar um controle adequado. Finalmente, o terceiro objetivo deste estudo é avaliar os efeitos de uma variação repentina da radiação solar no grau de superaquecimento. Dados experimentais foram utilizados para validação do modelo. Após validação, o modelo foi utilizado para realizar diversas simulações. Os resultados mostraram que uma pequena variação na radiação solar produz uma variação significativa no grau de superaquecimento, demandando uma ação imediata do dispositivo de expansão. Conclui-se então, que uma válvula de expansão eletrônica poderia ser o dispositivo de expansão mais indicado para regular a vazão mássica de CO_2 na entrada do evaporador. Ressaltando-se que ainda, a operação em continuo regime transiente em algumas estações do ano reforça a indicação da válvula eletrônica.

Palavras-chave: Bomba de Calor, Assistida por energia solar, CO_2, Resposta Dinâmica, Expansão direta.

LIST OF FIGURES

LIST OF TABLES

ABBREVIATIONS

COP	Coefficient of performance
CFC	Chlorofluorocarbons
CO_2	Carbon dioxide
DX-SAHP	Direct-expansion solar-assisted heat pump
DX-SAHPWH	Direct-expansion solar-assisted heat pump water heating
EEV	Electronic expansion valve
EPE	The Brazilian Energy Research Enterprise (Empresa Brasileira de Pesquisas Energéticas)
ESC	Etremum seeking control
GREA	Group of Refrigeration and Heating
GWP	Global warming potential
HFC	Hydro-fluorocarbons
HSR	Higher solar radiation
KTH	Royal Institute of Technology
LSR	Lower solar radiation
MAE	Maximum absolute error
ODP	Ozone depletion potential
PI	Proportional-integral
PID	Proportional-integral-derivative
PWM	Pulse width modulation
RMSE	Root mean square error
UFMG	Federal University of Minas Gerais – Universidade Federal de Minas Gerais

NOMENCLATURE

Special symbols

$\dot{m}$	Mass flow rate [$kg.s^{-1}$]
$\dot{Q}$	Heat transfer [W]
ΔTs	Superheat [°C]
$(dP/dZ)_{fr}$	Refrigerant pressure loss by friction [Pa]

Greek and special symbols

α	Void fraction
η	Efficiency, Compressor thermal efficiency
θ	Inclination of the absorber relative to the horizontal
ρ	Density [$kg.m^{-3}$]

Latin symbols

A	Area, plate area [m²]
C	Orifice coefficient
c_p	Specific heat at constant pressure [$J.kg^{-1}.K^{-1}$]
CO_2	Carbon dioxide
D	Diameter [m]
e(t)	Error during the time
e(kT)	Current error
e(kT-T)	Error in the previous instant of time
F	Fin efficiency
g	Acceleration of gravity [$m.s^{-2}$]
G	Mass flux [$kg.s^{-1}.m^{-2}$]
h	Specific enthalpy [$kJ.kg^{-1}$]
H_f	Heat transfer coefficient between the wall and the refrigerant [$W.m^{-2}.K^{-1}$]
K	Gain
L	Coil length [m]
n	Number of points
N	Rotation speed [rps]
p	Perimeter [m]
P	Pressure [Pa, bar]
S	Solar radiation [$W.m^{-2}$]
t	Time [s]
T	Temperature [K], discrete time
u	Controller output
u(kT)	Controller output in the current time
u(kT-T)	Controller output in the previous instant of time
u_{xi}	Standard uncertainty evaluated
u_y	Combined standard uncertainty
U_L	Combined coefficient involving radiation and convection between the absorber / coil and the environment [$W.m^{-2}.K^{-1}$]
v	Specific volume [$m^3.kg^{-1}$]
V	Volumetric displacement [$m^3.rev^{-1}$]
x	Quality, quantity analyzed
y	Dependent variable, function given
W	Distance between the centers of two adjacent tubes [m]

Common subscripts

c	Gas cooler outlet
CO	Compressor
d	Derivative
evap_model	Evaporating in model

evap_exp	Evaporating in experimental test
evap	Evaporating
exp	Experimental
f	Refrigerant
GC	Gas cooler outlet, gas cooler
i	Inner, inlet, integral, current, internal, interface
I	Integration
L	Liquid phase
o	Outer, outlet, external
orf	Cross-section needle valve orifice
p	Proportional
set	Correct value
sh	Superheat
sky	Sky
sup	Superheat
v	Volumetric, vapor phase
w	Water, tube wall
wi	Water intlet temperature
wo	Water outlet temperature
1	Compressor suction, evaporator / collector outlet
2	Compressor discharge, gas cooler inlet
3	Gas cooler outlet, expansion device inlet
4	Expansion device outlet, evaporator / collector inlet

Common Superscripts

0	Initial value

TABLE OF CONTENTS

1 INTRODUCTION

1.1 Background

A sustainable development requests energy production through renewable sources, better efficiency in energy conversion and proper use by users. The Brazilian Energy Research Enterprise (Empresa Brasileira de Pesquisas Energéticas - EPE) presented that in Brazil, 81.7% of the electricity in 2016 was produced through renewable energy sources (EPE, 2017). Furthermore, 21.4% of the electricity in 2016 was used for residential purposes. The Eletrobrás PROCEL (VASCONCELLOS and LIMBERGER, 2012) showed that in Brazil, 24% of the residential electricity consume occurs in the electric shower. Then, alternatives to produce hot water in Brazil have played an important role in the energy sector and, in this context, the employment of heat pumps have been highlighted as a more efficient option. The use of heat pump for water heating reduces the electricity consumption because this equipment uses thermal energy available in the environment. In a vapor compression cycle, the heat pump extracts heat energy from the environment and transfers it to the water, for example. To enable this energy transfer, a power input is required in the compressor. The hot water could be used at any time of the day. However, its production can be made at any other time, such as the period out of peak time when the consumption of electricity is higher in the Brazilian cities. Also, the production should preferably take place at times with higher thermal energy available in the environment. This scenario leads the system to operate with a higher coefficient of performance (COP).

Nowadays, for residential purpose, the use of heat pumps for water heating have not been widely used in Brazil. To be adequate for using, the water needs to be heated around 45°C, for direct consumption (SHAO *et al.*, 2004), and above 60°C, for storage (ASHRAE, 2000). It requires a control system of water temperature. Consequently, the temperature of the refrigerant in the condenser/gas cooler needs to be higher than the hot water temperature. However, the operation of the heat pump with high temperatures in the condenser/gas cooler leads to a degradation of the COP. To meet these requirements and operate with good performance, different solutions have been used in heat pumps. The solar-assisted systems are one of them (CHUA; CHOU; YANG, 2010; HEPBASLI; KALINCI, 2009).

Among the solar-assisted systems, the Direct-Expansion Solar-Assisted Heat Pump (DX-SAHP) is one of the technologies used to produce hot water (HEPBASLI; KALINCI, 2009;

OMOJARO; BREITKOPF, 2013). In a DX-SAHP the evaporator/collector receives energy from the atmospheric air and from solar radiation. For these systems, the rise of solar radiation results in an increase of the heat pump COP (MOHAMED *et al.*, 2017; KONG; SUN; *et al.*, 2018).

Besides, an important role in the refrigeration system is to select an environment-friendly refrigerant (CALM, 2008; MOHANRAJ; JAYARAJ; MURALEEDHARAN, 2009; SARBU, 2014; DUARTE, 2018). Different refrigerants such as chlorofluorocarbons (CFCs), hydro-fluorocarbons (HFCs), natural refrigerants and hydrocarbons have been used in the heat pumps. Actually, there are mandatory requirements to select a refrigerant. The current international agreements, including the Montreal (UNEP, 1987) and Kyoto (GECR, 1997) Protocols to prevent stratospheric ozone depletion and global climate change, respectively. One of the refrigerants that meet these requirements is the carbon dioxide (CO_2). CO_2 is a natural refrigerant with zero ODP (ozone depletion potential) and GWP (global warming potential) equal to one. Also, CO_2 has been used extensively in the heat pump to produce hot water (MA; LIU; TIAN, 2013) and it allows the heat pump to operate with a good performance (WILLEM; LIN; LEKOV, 2017).

A CO_2 DX-SAHP was built by the Group of Refrigeration and Heating (GREA) in the Department of Mechanical Engineering at the UFMG (Universidade Federal de Minas Gerais), which is the only existing CO_2 DX-SAHP in Brazil, in the literature analyzed. In a CO_2 heat pump, using a basic cycle configuration, the expansion device controls the optimum high pressure (PÉREZ-GARCÍA *et al.*, 2013). In consequence, in this system, the superheat is not controlled. In a DX-SAHP, the fluctuation of solar radiation produces variation in the superheat (KONG; JIANG; *et al.*, 2018). In that way, it is important to verify the possibility to control the optimum high pressure instead of controlling the superheat in a CO_2 DX-SAHP, using a basic cycle configuration. Furthermore, the effects of sudden variations in the solar radiation on the superheat might be better understood. These are important steps to operate a small CO_2 DX-SAHP with good performance and safety.

1.2 Objectives

1.2.1 Main objective

The main objective of this investigation is to control a small carbon dioxide direct-expansion solar-assisted heat pump as a low-cost solution using a basic cycle configuration and to analyze the effect of solar radiation variation on the superheat.

1.2.2 Specific objectives

The specific objectives are:

- to design and implement the control system to adjust the hot water outlet temperature according to the water mass flow rate, regardless of the ambient conditions and operational parameters of the heat pump;
- to develop an experimental evaluation if there is a specific internal area of the expansion device that leads the system operation near to the optimum high pressure with an acceptable superheat;
- to evaluate the effects of the solar radiation variation, through a distributed mathematical model, in the superheat.

1.3 Outline of the Thesis

This thesis is divided into the following 6 chapters:

- Chapter 1 states the motivation and background for this work, and also the objectives;
- Chapter 2 contains a review of literature and describes relevant scientific works that have a direct relation with the theme of this thesis;
- Chapter 3 presents the description of the experimental setup;
- Chapter 4 describes the methods used in this thesis;
- Chapter 5 presents the results of this investigation;
- Chapter 6 provides conclusions.

The major contributions of the thesis are linked to the papers listed in Appendix A.

2 LITERATURE REVIEW

2.1 CO_2 as a refrigerant

The "natural" refrigerants, such as, ammonia, carbon dioxide and sulfur dioxide, had been widely used between 1850 and 1930. After that, the CFCs and HCFCs (Hydrochlorofluorocarbons) emerged as a safer and environmentally friendly refrigerants. Then, the natural refrigerants have become obsolete, except for ammonia (LORENTZEN, 1994). However, in 1974, Molina and Rowland (MOLINA; ROWLAND, 1974) presented a work that demonstrated that the emissions of chlorine caused damage to the ozone layer. Subsequently, several countries by the Montreal Protocol agreed to replace substances that have ozone depletion potential (ODP). In consequence, HFCs started to be used. Nowadays, in addition to zero ODP, it is necessary for refrigerants to present low global warming potential (GWP) to be considered environmentally friendly (CALM, 2008). The greenhouse gases control was proposed in the Kyoto protocol.

At the beginning of 1990s, CO_2 as a refrigerant started to be reused as a result of the environmental issues and because of the patent application for a transcritical CO_2 automotive air conditioning published by Gustav Lorentzen (LORENTZEN, 1990). This theory solved the problem of the capacity and efficiency loss near to the critical temperature. Currently, the main applications of CO_2 as a refrigerant are: automotive air conditioning; heat pumps for water heating and commercial refrigeration system, usually using cascade solutions (MA, LIU and TIAN, 2013).

CO_2 is (a) available in large quantities in the atmospheric air; (b) it has zero ODP; (c) the GWP is one; (d) it is non-flammable; (e) it is not explosive; (f) it has high volumetric performance which allows the use of smaller compressors and heat exchangers; (g) low pressure loss. The major drawback of CO_2 transcritical system is the high pressure, which requests robust components. However, the current technological development has overcome this problem (PEARSON, 2005). Another drawback is the difficulty in identifying a leak because CO_2 is denser than atmospheric air and have no odor.

2.2 Heat pumps

Typical applications of heat pumps are water and air heating for residential, commercial and industrial purpose (GRANRYD, 2005). The main heat pump components are evaporator, compressor, condenser/gas cooler and expansion device. The heat exchanger that operates with the heat source is called condenser in a subcritical cycle because of the condensation process and

gas cooler in a transcritical cycle because the heat transfer occurs only due to sensible heat. The pressure-enthalpy diagram for a subcritical and transcritical cycle are presented in Fig 1 (a) and Fig. 1 (b), respectively. In transcritical cycle the heat rejection occurs above of the critical temperature.

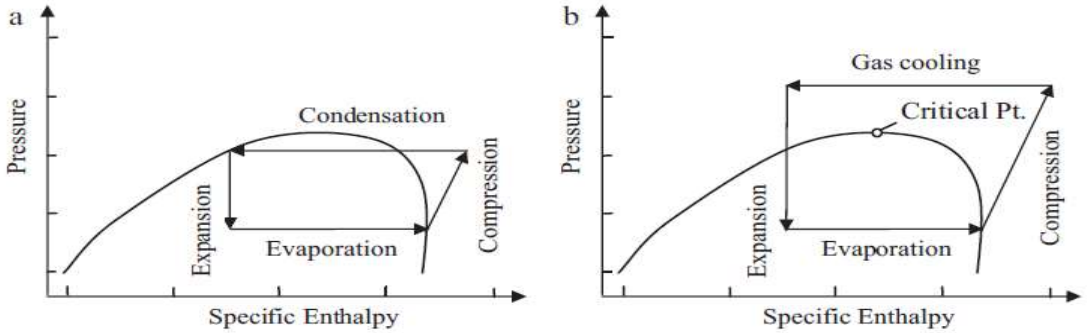

FIGURE 1 – Pressure-enthalpy diagram: (a) subcritical; (b) transcritical
Source: Austin and Sumathy, 2011.

In CO_2 heat pump, the vapor compression cycle operates in two different manners. Firstly, in a subcritical cycle, and secondly, few seconds after the start-up, in a transcritical cycle. Before the start-up, the temperature of CO_2 is equal to the room temperature. Consequently, the system pressure is around 60 bar. Then, the compressor is turned on. At that time, the operation occurs in subcritical cycle, as shows Fig. 1 (a). The pressure in evaporator is reduced and the pressure in condenser/gas cooler is increased. When the pressure in the condenser/gas cooler is above 70 bar (73.8 bar and 31°C) the operation occurs in transcritical cycle, as shown Fig. 1 (b).

2.2.1 The use of CO_2 in heat pumps

Heat pumps working with CO_2 have been widely manufactured. This type of equipment is called Eco Cute (name emerged in Japan in the 1990s) and they have been commercialized intensively since 2001. In the Japanese market, until 2011, the cumulative sales of Eco Cute reached more than three million units (ZHANG, QIN and WANG, 2015). It was also sold in other Asian countries, in Europe and in the United States. They are manufactured, for example, by Denso, Panasonic, Sanden, Toshiba Carrier and Hitachi.

Even with the large-scale production, CO_2 heat pump is a technology that needs efforts to improve its performance. A comprehensive literature review about CO_2 transcritical cycles configurations was presented by Pérez-García *et al.* (2013). The authors presented six different system configurations. The first one is the basic configuration, as shows Fig. 2. In this

configuration the expansion device acts to operate the system with optimum high pressure. Subsequently, in the topic 2.3.1, it will be explaining the importance of operating the transcritical CO_2 system near to the optimum high pressure. The second configuration includes an additional expansion device to control the superheat and modify the position of the liquid receiver, as presents Fig. 3. According to the authors the second configuration improve the performance of the cycle.

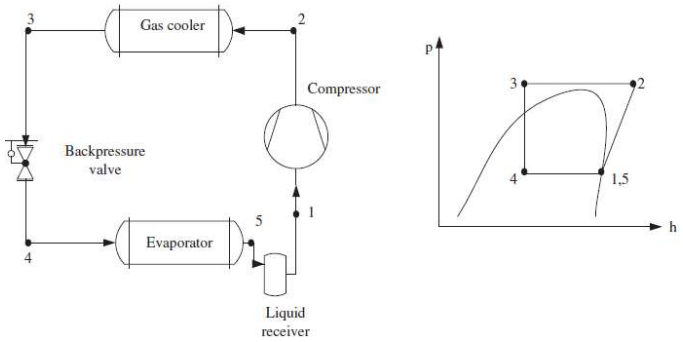

FIGURE 2 – Basic cycle configuration.
Source: Pérez-García *et al.*, 2013.

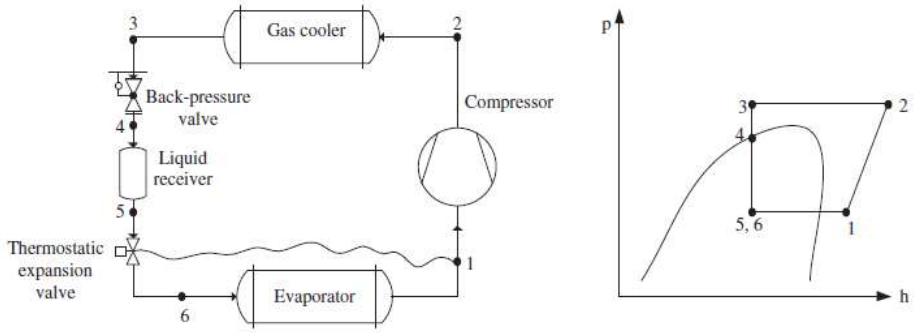

FIGURE 3 – Dual expansion device configuration.
Source: Pérez-García *et al.*, 2013.

In that way, all of the following configurations improve the performance of CO_2 transcritical cycle. The third configuration adds an internal heat exchanger between the gas cooler and expansion device in a basic cycle. This change increases the subcooling degree at the gas cooler outlet. The fourth configuration adds an internal heat exchanger between the gas cooler and the back-pressure valve in a dual expansion device configuration. The fifth configuration replaces the expansion device to an expansion work recovery. This solution takes advantage of the available energy in the transcritical CO_2 system due to the large pressure difference between the evaporator and the gas cooler. Finally, the sixth configuration adds an internal heat exchanger in an expansion work recovery cycle.

2.2.2 Direct expansion solar assisted heat pump (DX-SAHP)

In a DX-SAHP the evaporator is also the solar collector. The DX-SAHP receives besides of the energy from natural and forced convection as well as from the condensation of water vapor in the external atmospheric air, the energy from solar radiation. This highest energy input is shown in Fig. 4 and it also increases the evaporating temperature and pressure. The increase of the COP in a DX-SAHP is presented in the literature (ITO, MIURA and WANG, 1999; KONG *et al.*, 2011; SUN *et al.*, 2014). Furthermore, DX-SAHP operates with better COPs than a non-solar assisted heat pump (SUN *et al.*, 2015).

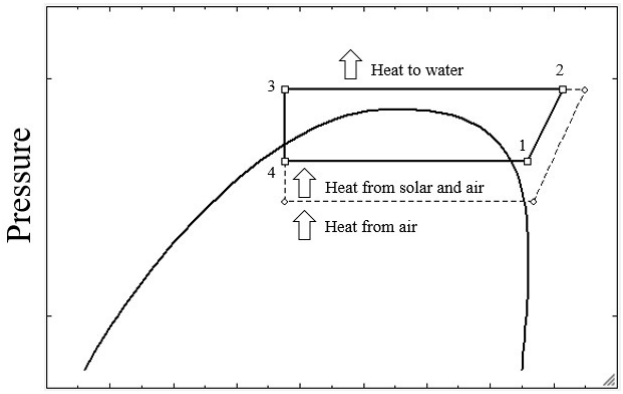

FIGURE 4 – Low pressure increase in a CO_2 DX-SAHP.
Source: Adapted from Sun *et al.* (2014).

Omojaro and Breitkopf (2013) reported that 75% of the works about DX-SAHP were done to water heating. Different refrigerants have been used in a direct expansion solar assisted heat pump water heating (DX-SAHPWH), such as: R12 (CHATURVEDI and ABAZERI, 1987; CHATURVEDI, CHEN and KHEIREDDINE, 1998; ITO, MIURA and WANG, 1999), R22 (LI *et al.*, 2007; KARA, ULGEN and HEPBASLI, 2008; KONG *et al.*, 2011), R134a (MORENO-RODRIGUEZ *et al.*, 2013; SUN *et al.*, 2014; KONG; SUN; *et al.*, 2018), R744 (ISLAM *et al.*, 2012; FARIA *et al.*, 2016), R410A (KONG *et al.*, 2017) and R407C (MOHAMED; RIFFAT and OMER, 2017).

2.3 Control of CO_2 transcritical systems

2.3.1 Control of the optimum high pressure in CO_2 transcritical systems

This topic has been inserted to present the importance of the optimum high-pressure control. This is the main strategy adopted in a great number of the works related with the control of CO_2 systems. Topics 2.3.2 and 2.3.3 will present some of these works.

Liao, Zhao and Jakobsen (2000) discussed that in a subcritical system a reduction in the high-pressure results in an increase of the COP. However, in the gas cooler, the temperature and pressure are independent. Then, there is an optimum high pressure for which the COP is maximum. They explained it through Fig. 5. The rise of high-pressure (P_c) results in an almost linear increase in the compression work (w). However, the cooling capacity (q) increase rapidly to gas cooler outlet pressure up to about 90 bar and it rises relatively slow to gas cooler outlet pressure above to about 90 bar, as shows Fig. 5 for the simulation conditions presented by the authors. This fact leads to a maximum COP due to an optimum high-pressure. The experiment was carried out with an evaporating temperature of 10°C, a CO_2 gas cooler outlet temperature of 40°C and a superheat of 5°C.

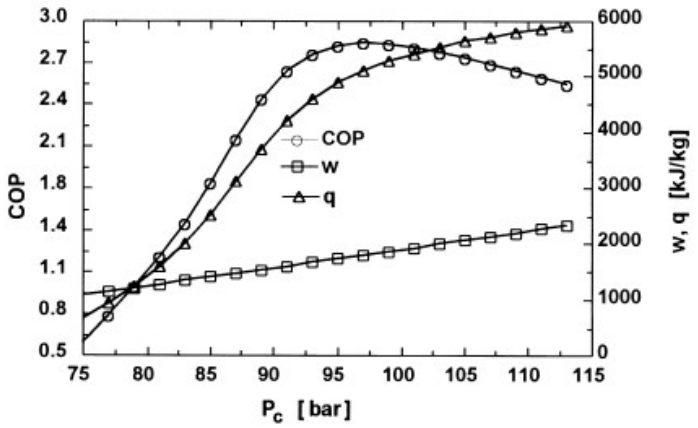

FIGURE 5 – The effect of high pressure on the cooling capacity, the compression work and the COP.
Source: Liao, Zhao and Jakobsen, 2000.

A comprehensive literature review of the optimum high pressure was developed by Yang *et al.* (2015). The authors presented that the optimum high pressure is obtained as a function of CO_2 gas cooler outlet temperature, the evaporating temperature, and the compressor isentropic efficiency. Moreover, they highlighted the gas cooler outlet temperature as the most relevant factor.

The variations of COP with the high pressure for different evaporating temperature (T_{evap}) and gas cooler outlet temperature (T_{GC}) are shown in Fig. 6. It is possible to notice that there is an optimum high pressure for each CO_2 gas cooler outlet temperature. The rise of CO_2 gas cooler outlet temperature reduces the COP and increases the optimum high pressure. Also, an optimum high pressure is observed in the evaporating temperatures curves. The increase of the evaporating temperature produces a rise of the COP and small effects in the optimum high pressure.

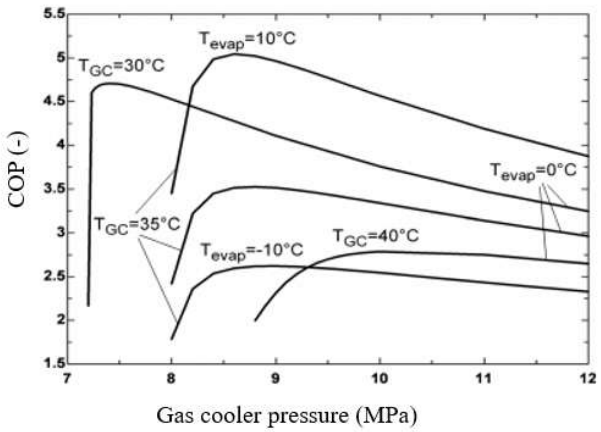

FIGURE 6 – COP versus Gas cooler pressure for different evaporating and gas cooler outlet temperatures.
Source: Groll and Kim (2007).

Different correlations were presented in the literature to calculate the optimum high pressure. There are correlations that consider: (i) the gas cooler outlet temperature or ambient temperature (CHEN and GU, 2005; ZHANG, et al., 2010; QI et al., 2013); (ii) the gas cooler outlet temperature and the evaporating temperature (LIAO, ZHAO and JAKOBSEN, 2000; SARKAR, BHATTACHARYYA and GOPAL, 2004; YANG et al., 2015); (iii) the gas cooler outlet temperature, the evaporating temperature and the compressor isentropic efficiency (APREA and MAIORINO, 2009); and (iv) the water temperature (SARKAR, BHATTACHARYYA and GOPAL, 2006; WANG et al., 2013).

2.3.2 Control in CO_2 refrigeration systems

Aprea and Maiorino (2009) developed a study to determine a correlation of optimum high pressure in a Split CO_2 system. The main components of the equipment are: (i) a semi-hermitic two-stage compressor; (ii) an oil separator; (iii) a gas cooler; (iv) a receiver; (v) an evaporator; (vi) a backpressure electronic expansion valve to regulate the optimum high pressure; and (vii) an

electronic expansion valve to regulate the superheat. As described in section 2.3.1, the proposed correlation considers the gas cooler outlet temperature, the evaporating temperature and the compressor isentropic efficiency and the correlation was adjusted from Liao, Zhao and Jakobsen (2000). The results showed that for each ambient temperature the control system can lead the system to operate in the optimum high pressure.

A real time optimum high pressure control method was presented by Kim, Shin and Kim (2014). The main components of the equipment are: (i) a compressor driven by frequency inverter; (ii) an electronic expansion valve driven by a step motor; (iii) a gas cooler; (iv) an evaporator; and (v) an internal heat exchanger. The user sets the cooling capacity and a PI (proportional - integral) control act in the compressor frequency inverter to achieve this value. Other PI controller acts to open the expansion valve. The methodology considered a small increase in the gas cooler pressure due to the small reduction of the internal area of the expansion device. It led to the increase of power consumption of the compressor and cooling capacity. Then, it was checked if the COP increase or decrease. The optimum high-pressure values achieved through the proposed methodology were similar to the values presented by the methodologies that do not work in real time.

Salazar and Méndez (2014) proposed a theoretical study about the control of the outlet temperatures in the evaporator and gas cooler in a transcritical CO_2 cycle. The main components of equipment are: (i) a compressor; (ii) an expansion valve; (iii) a gas cooler; and (iv) an evaporator. From a lumped energy balance, they analyzed a linear and a non-linear model. The PID (proportional-integral-derivative) control was the technique used in the linear system, and a commercial numerical code was the technique used in the non-linear system. The evaporator control was carried out considering it as an isothermal device and the gas cooler control was performed considering the outlet CO_2 temperature. The results showed better stability for the evaporator but its control was dependent on the gas cooler control. The comparison among the linear and non-linear systems presented a similar behavior. However, the linear method showed an easier stabilization.

Peñarrocha *et al.* (2014) proposed a real-time optimization method to operate CO_2 transcritical refrigeration systems. The control strategy sought to minimize the compressor energy consumption. The methodology was mathematically demonstrated and validated in an ice production plant. The main components are the semi-hermetic compressor, two expansion devices

(a back-pressure valve to regulate the optimum high pressure and an electronic expansion valve to regulate the superheat), two counter-current concentric heat exchangers (evaporator and gas cooler). The measurements carried out were the compressor electric consumption, CO_2 gas cooler outlet pressure and the water temperature in the evaporator. During the experiments the water mass flow rate and the water inlet temperature in the evaporator were modified. Two PI controllers were implemented in the system. The first one to control the compressor speed by means of a frequency inverter, and the second to regulate the back-pressure valve opening area through a step motor. The authors highlighted the low instrumentation required to control the system, which makes easy to replicate control system in other equipment. The results showed a reduction in the energy consumption and an improvement in the COP.

2.3.3 Control of CO_2 heat pump systems

Minetto (2011) presented a control system to maximize the COP of CO_2 heat pump. The main components of the system are an one-stage compressor, a coaxial gas cooler, an electronic expansion valve, two parallel finned tube evaporators, an internal heat exchanger and a receiver. A PID control was used to regulate the water mass flow and maintain the set point of the outlet water temperature. The control system acted to adjust water mass flow rate and maintain the set point of the water outlet temperature. At the same time, the control logic estimated the real-time COP as a function of compressor discharge and suction pressures, gas cooler outlet temperature and suction temperature. The second one control system opens the expansion valve. The results showed that the water outlet temperature was near to the set point value with an average difference of 1.1°C. In addition, the water set point temperature was reached after 8 min of the startup. Furthermore, the authors recommended an adaptive control logic to achieve the optimum high pressure.

Baek *et al.* (2013) presented a work in which control methods to the gas cooler pressure in a CO_2 heat pump were tested. The alternatives were: (i) variation of the refrigerant charge; (ii) variation of the refrigerant mass flow rate through the electronic expansion valve; (iii) variation of the compressor speed; and (iv) variation of the fans speed installed near the evaporator and the gas cooler. The main components are the rotary compressor, the evaporator, the gas cooler, the electronic expansion valve and the oil separator. A step motor drove the electronic expansion valve. During the experiments, the superheat was maintained at 5°C. The gas cooler and evaporator

were kept at separated areas, in both places the temperature could change between -20°C and 50°C, and the relative humidity could vary between 0 and 100%. The presented the best operating point for each analyzed alternative. It showed that the reduction of the internal area of the expansion device resulted in an increase in the gas cooler pressure and in an increase in the cooling capacity. In addition, the increase in the fan speed resulted in a decrease in the gas cooler pressure. Furthermore, for a specific cooling capacity and compressor speed there was a specific optimum high pressure. Finally,

An experimental investigation on the optimum high pressure in a transcritical CO_2 heat pump was performed by WANG *et al.* (2013). For this purpose, they implemented a PID control for water outlet temperature. In the gas cooler, the water inlet temperature was kept at 12°C and the water outlet temperature was set between 55°C and 80°C. The set point of water outlet temperature was obtained by modifying the water mass flow rate. The results showed that CO_2 gas cooler outlet temperature and evaporating temperature influenced the optimum high pressure and COP.

Ge and Tassou (2014) carried out an optimum high-pressure study in a cascade CO_2 system. The control of the optimum high pressure was made by the back-pressure valve. The system was implemented in a software developed by the authors. The simulation was applied for UK supermarkets for the period of one year. In the cascade system the low-pressure part provided the thermal energy for the cold storage with medium and low temperature. The desired supermarket temperature should be kept between 18°C and 24°C. To achieve this set point, a ventilation system mixed recirculation and fresh air. After that, depending on the air temperature, the mixed air can be cooled or heated. The system was implemented to analyze if the heat pump could be able to heat the ambient air totally or partially. A gas system was the additional source in the cases of the energy available in the heat pump was not enough. When, the air temperature was above 25°C it was considered that the system operates in a transcritical cycle. To control the system, four options were analyzed: (i) for ambient temperature above 25°C, the four options considered that the gas cooler pressure could vary between 80 bar and 120 bar; (ii) for ambient temperature below 25°C, option 1 considered that the gas cooler pressure could change, option 2 and 3 considered a fixed value for the gas cooler pressure, at 60 bar and 70 bar, respectively, while option 4 considered that the gas cooler pressure could vary between 80 bar and 120 bar. The results showed that the increase of the high pressure implied in a higher heat recovery. However, the energy consumption of the compressor also increased. An economic analysis was carried out taking into account the current

prices of gas and electricity. It was concluded that option 1 was the best control strategy. Despite presenting the lowest heat recovery, it had the lowest energy consumption of the compressor.

Hu *et al.* (2015) proposed a mathematical model that use the methodology "extremum seeking control – ESC" (developed by Ariyur and Krstic in 2003). In this work, the simulated heat pump has a reciprocating compressor, an internal heat exchanger, an expansion device, an evaporator, and a receiver. The water circuit has a pump driven by a frequency inverter. The goal of the system was produced the desired water heating with the maximum COP for different ambient conditions. The methodology was tested in Modelica[1] software. Two PI control system were used. In the first one the outlet gas cooler pressure and COP were the input data and the desired variable, respectively. In the second one, the water pump speed and water outlet temperature were the input data and the desired variable, respectively. The results indicated a good performance in terms of error and steady state convergence time.

2.4 Control of DX-SAHP

The control of a R134a DX-SAHP is presented by Kong *et al.* (KONG; JIANG; *et al.*2018). They presented a control strategy able to keep the equipment with an adequate performance in different environment conditions. As the variation of solar radiation results in a regular transient operation, the authors choose an electronic expansion valve. This expansion device was suggested for transient systems by Aprea and Mastrullo (2002). Besides, of the electronic expansion valve the main components of the system are a hermetic compressor, a micro channel condenser and an evaporator/collector. The control strategy was used to keep the superheat between 5°C and 10°C.

Kong *et al.* (KONG; JIANG; *et al.*, 2018) discussed that during the startup of the system, the opening area of the expansion device is an important factor for the proper system performance. A large opening area may result in the liquid being carried over into the compressor although it will help to achieve the superheat setpoint quickly. On the other hand, a small opening area may require the operation of the system in an inappropriate condition for a long period. Then, they developed from experimental tests a correlation to calculate the initial opening area of the expansion device. This correlation is a function of the environment temperature and the solar radiation. Thus, before starting the compressor, the environment temperature and solar radiation are measured for 2

[1] https://www.modelica.org/ Modelica and the Modelica Association. Accessed in 10/07/15 – 15:14.

minutes. After that, the compressor is turned on and the correlation adjust the opening area of the expansion device. After 5 minutes, other equations proposed by the authors are used to keep the superheat between 5°C and 10°C.

The variations of superheat (t_{sup}) with time (τ) are presented in Fig. 7 for three different days. It can be noticed that the majority of points are between 5°C and 10°C as defined in the controller requirements. There are points out this range in December 19th, according to the authors it is occurring due to the solar radiation variation in this day.

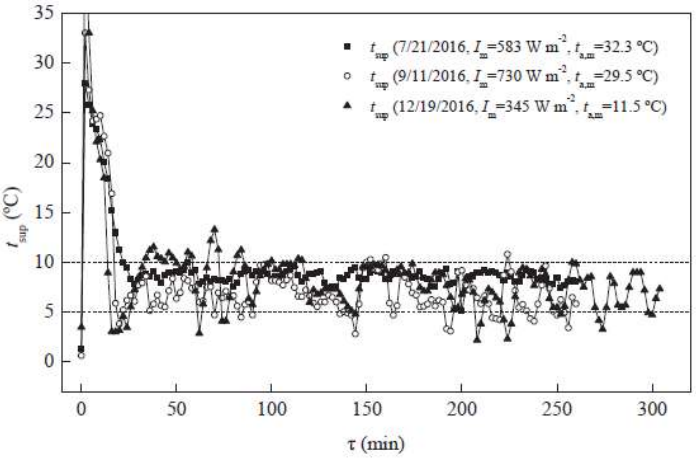

FIGURE 7 – Variations of superheat with time.
Source: Kong *et al.* (KONG; JIANG; *et al.*, 2018).

2.5 Influence of opening area of the expansion device on the performance of transcritical CO_2 system

The influence of opening area of the expansion device in a CO_2 heat pump was investigated by WANG *et al.* (2013), as presented by Fig. 8. The main system components are a compressor, a counter current gas cooler, an internal heat exchanger, an evaporator and two expansion devices to achieve better precision. The test was carried out with steady state conditions in the gas cooler and evaporator. A PID control kept the water outlet temperature in the correct value. In the Fig. 8, the direction of the arrows shows the reduction of the internal area of the expansion device between the two cycles. It can be noticed that a reduction in the internal area of the expansion device results in an increase of gas cooler pressure and a decrease of evaporating pressure. In addition, when the internal area is reduced, CO_2 mass flow rate decreases. In consequence, the superheat increases and CO_2 gas cooler outlet temperature decreases.

A comprehensive experimental investigation of the influence of the opening area of the expansion device was presented by Hou *et al.* (2014). The main system components are a semi-

hermetic reciprocating compressor, a gas cooler, an electronic expansion valve, an evaporator, a receiver and an oil separator. During the tests, the water inlet temperature was 30°C in the gas cooler and 15°C in the evaporator.

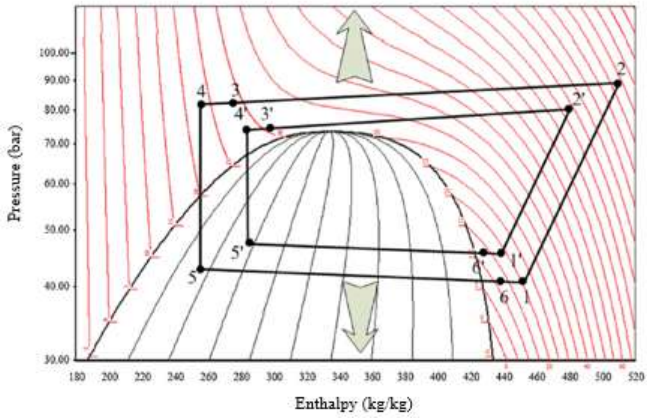

FIGURE 8 – Variations of gas cooler and evaporating pressure with reduction of expansion device area.
Source: WANG *et al.* (2013).

The results showed that an increase in the internal area of the electronic expansion valve (EEV) produced a decrease in the discharge pressure and in the outlet gas cooler pressure. At the same time produced a little variation in the compressor inlet pressure, as shown Fig. 9. According to the authors, the variation in the compressor inlet pressure occurs because the evaporating pressure is strongly dependent on the heat transfer in the evaporator. Moreover, during the tests the heat transfer remained constant. The results presented by Hou et al. (2014) for the variation of suction pressure due to the opening area of the expansion device are different from those presented by WANG et al. (2013).

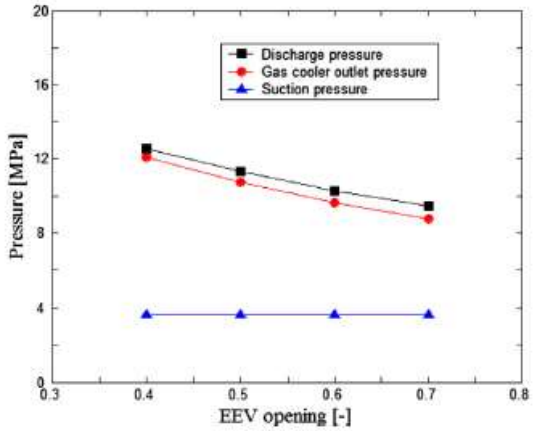

FIGURE 9 – Variations of the pressures with EEV opening.
Source: Hou *et al.* (2014)

The effects of the opening area of the expansion device in temperatures are presented in Fig. 10. It can be seen a reduction in the compressor discharge temperature and small increases in the gas cooler outlet temperature and in the evaporating temperature. However, the evaporating temperature remains almost constant. As previously discussed, the behavior of evaporating temperature is different from that presented by WANG *et al.* (2013).

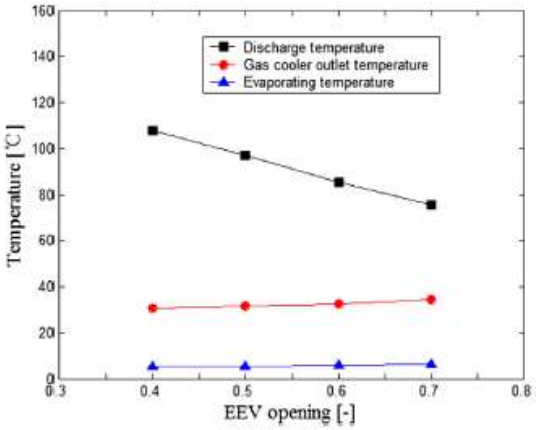

FIGURE 10 – Variations of temperatures with EEV opening.
Source: Hou *et al.* (2014)

Furthermore, the variation of the internal area of the expansion device from 40% to 70% produced an almost linear increase in CO_2 mass flow rate. As shows Fig. 11, when the internal area of the expansion device is 40% and 70% the CO_2 mass flow rate is 0.149 kg/s and 0.184 kg/s, respectively.

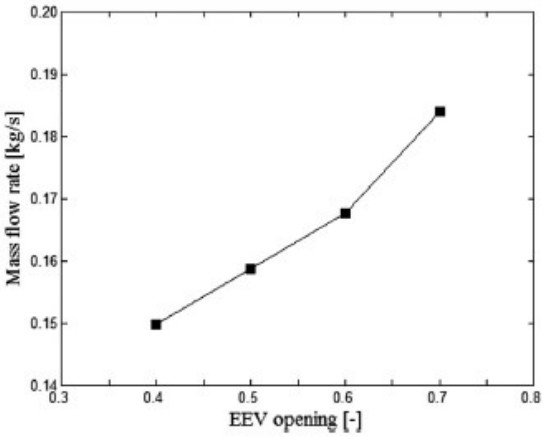

FIGURE 11 – Variation of mass flow rate with EEV opening.
Source: Hou *et al.* (2014)

The influence of the opening area of the expansion device in the COP is presented in Fig. 12. It is shown that there is an opening area in which the system operates with maximum COP. This opening area match to the optimum high pressure.

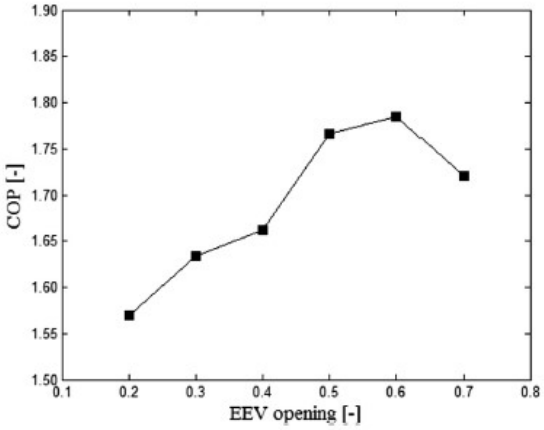

FIGURE 12 – Variations of the system COP with EEV opening.
Source: Hou *et al.* (2014)

2.6 Effects of superheat

2.6.1 Effects of superheat in a transcritical CO_2 system

The effect of superheat (tsh) in a transcritical CO_2 system is analyzed in Fig. 13 by Liao; Zhao and Jakobsen (2000). During the tests, the evaporating temperature and the gas cooler outlet temperature were set at 10°C and 35°C, respectively. The analysis was carried out for three different gas cooler outlet pressure (P_c). It is noted that in the analyzed gas cooler outlet pressure the variation of the superheat almost did not produce changes in the COP. Equally, Zhang *et al.* (2010) and WANG *et al.* (2013) reported that the superheat has little influence in the optimum high pressure.

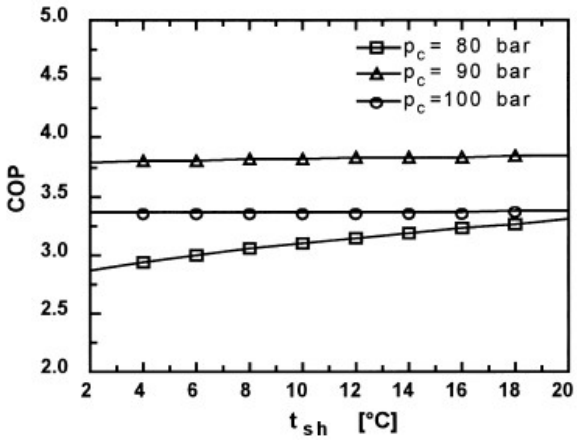

FIGURE 13 – Superheat effects in COP for different gas cooler pressures.
Source: Liao; Zhao and Jakobsen, 2000.

2.6.2 Effects of superheat in a DX-SAHP

Despite of the operation of a DX-SAHP with higher COP, as discussed in topic 2.2.2, this type of equipment is more influenced by environmental conditions than a non-solar assisted heat pump. On a typical day occurs variations in the ambient temperature, solar radiation and wind speed, and these are environmental conditions that affect the DX-SAHP performance (XU; ZHANG and DENG, 2006; KONG *et al.*, 2011; SUN *et al.*, 2014). However, the solar radiation variation is the most extensive of them and it could occur instantaneously. The solar radiation variation changes the refrigerant properties such as evaporating temperature (KONG *et al.*, 2011) and superheat (KONG; JIANG; *et al.*, 2018). For example, the system is operating in a steady state condition. At this moment, a cloud covers the evaporator / collector and the solar radiation does not achieve it directly. Then, the entrance of energy in the evaporator / collector is reduced and consequently the superheat reduces. Variations of solar radiation occur in both directions and it results in an increase or a decrease of superheat. Kong *et al.* (KONG; JIANG; *et al.*, 2018) reported superheat variations due to the solar radiation changes.

The effects of the superheat variations may be harmful to the system. The increase in superheat may result in the degradation of lubricant oil as well as it makes the properly cool of the electric motor more difficult, in a hermetic compressor. On the other hand, the decrease in superheat may result in the liquid being carried over into the compressor.

2.7 Final Comments of literature review

Based on the literature review, it was observed a significant number of theoretical and experimental studies of DX-SAHP, operating with different refrigerants. Several works also assessed the non-solar assisted CO_2 heat pumps. Although, there are few works about CO_2 DX-SAHP and none of them discuss the effects of the expansion device opening (FARIA *et al.*, 2016; OLIVEIRA *et al.*, 2016). Kong *et al.* (KONG; JIANG; *et al.*, 2018) highlighted the importance of the expansion device in a R134a DX-SAHP to keep the superheat in the correct value. Since solar radiation can vary considerably during the day, these fluctuations can introduce important changes in the evaporating temperature and the superheat.

Furthermore, there are studies that discuss the variation of the evaporating temperature and superheat due to the variation in the solar radiation. However, there are no experimental and numerical studies that investigates the superheat dynamics when the solar radiation changes.

3 EXPERIMENTAL DEVICE

3.1 Experimental set up

The DX-SAHP was designed to produce hot water and CO_2 was the refrigerant used. The basic components are the compressor, the gas cooler, the needle expansion valve and the evaporator / collector as shows Fig.14. The compressor is manufactured by SADEN (model SRCaDB). It is a hermetic reciprocating with constant speed, a displacement of 1.75cm ^{3}/rev, it is driven by two poles asynchronous electric motor powered in 127V, and 60Hz. Swagelok manufactures the expansion valve (model SS-31RS4). It is a needle valve with a diameter orifice of 1.6 mm. The data of the countercurrent concentric gas cooler is presented in Tab. 1 and the data of the evaporator / collector is presented in Tab. 2.

The other components of the DX-SAHP are: (i) the oil separator manufactured by Temprite (model 131) with a maximum working pressure of 160 bar and the oil return to the compressor is done manually through a valve; (ii) the receiver with an inner volume of 1.22 liters; (iii) the filter drier; (iv) the small pump used to delivery cold water, the water pump data are presented in Tab. 3; (v) a cold water tank with 20 liters; (vi) a tank with 200 liters used to store hot water for consumption. These components are also presented in Fig. 15.

FIGURE 14 - Experimental device of CO_2 DX-SAHP.

TABLE 1 – Gas Cooler Parameters.

Type	Countercurrent concentric
Tube Material	Cooper
Refrigerant	CO_2
Secondary fluid	H_2O
CO_2 diameter (outer / inner)	D_o = 6.34 mm / D_i = 4.66 mm
Water diameter (outer / inner)	D_o = 12.7 mm / D_i = 12 mm
Total length of tube	24.3 m

Source: Modified by Oliveira (2013), p. 61.

TABLE 2 – Evaporator / collector Parameters.

Type	Direct-expansion solar assisted
Material of the tube and fin	Cooper
Refrigerant	CO_2
Secondary fluid	Atmospheric air
CO_2 diameter (outer / inner)	D_o = 6.34 mm / D_i = 4.66 mm
Total length of the tube	16.3m
Fin thickness	1 mm
Fin efficiency (Project data)	0.98
Inclination to the horizontal	25°
Collector area	1.57 m²

Source: Modified by Faria (2013), p. 66.

TABLE 3 – Small Water Pump Parameters.

Manufactured	SHURflo
Model	100-000-21
Volumetric flow rate	1.0 L/min
Pressure	0.7 bar
Voltage	12 VDC
Maximum current	2.4 A
Note	Requires the installation of a 3.0A fuse in the power supply

3.2 System monitoring

Five T-type thermocouples with accuracy of 0.5°C were installed at the inlet and outlet of each component to measure the temperatures. All thermocouples were located outside the copper pipe. Three FuelTech pressure sensors with accuracy of 0.5% (from 0 to 102 bar) were used to measure the pressure at the compressor suction, compressor discharge, and gas cooler outlet. A ZURICH mechanical pressure gauge installed at the compressor suction with accuracy of 0.25%

(from 0.1 to 200 bar) was employed to measure the low pressure of the system. A power meter model ETP 30 from ABB with accuracy ±5% and range of 0 to 1039 W was used to measure the power consumed in the compressor. Two BLACK & WHITE pyranometers model 8-48 (±5%, range spectral 295 to 2800nm) were used to measure the solar radiation flux, one fixed at the same inclination of the solar collector and other at the horizontal plane. CO_2 mass flow rate was calculated by energy balance in the gas cooler. The uncertainty of these variables was calculated by the BIMP (JOINT COMMITTEE FOR GUIDES IN METROLOGY, 2008) method described in the Eq.1. Where u_y is the combined standard uncertainty, u_{xi} is the uncertainty of each variable, y is the function given, x is the quantity analyzed, and N is the number of variables. All measuring instruments have been properly calibrated.

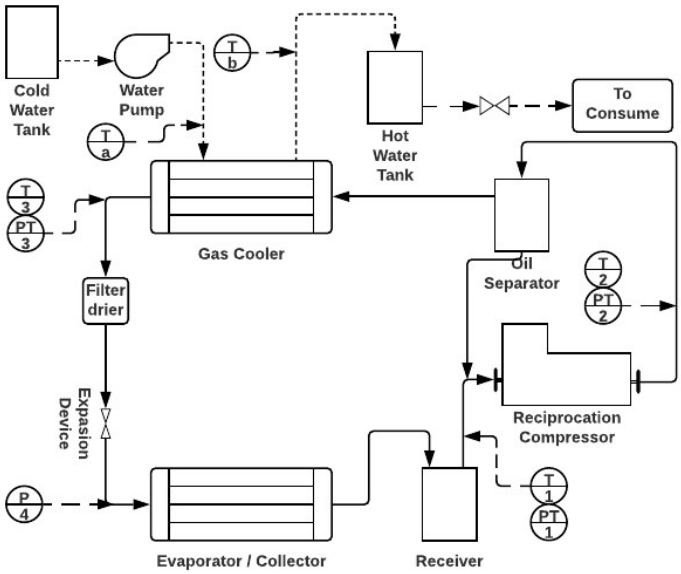

FIGURE 15 – Schematic of the experimental device of the DX-SAHP operating with CO_2.

$$u_y^2 = \pm \sum_{i=1}^{N} \left(\frac{\partial y}{\partial x_i} u_{xi} \right)^2 \quad (1)$$

The acquisition board used were manufactured by National Instrument. The thermocouples are connected to the acquisition board USB-9162 while the others data are acquired by the acquisition board USB-6211. A Labview program is used to monitor and record all data. The Matlab with Coolprop toolbox software is used to calculate the thermodynamic parameters. In

Fig.15 the numbers 1, 2, 3 and 4 are CO_2 cycle position and the letters a and b are the water inlet and outlet in the gas cooler, respectively.

3.3 Water heating control system

The control of the water heating could be developed through a Labview program, a programmable logic controller or by an embedded system. Considering that this type of heat pump is designed to be used in residences, the cost is an important factor. Then, the embedded system was chosen. Table 4 shows the electronic components list used to control the water heating.

TABLE 4 – Electronic components list.

Item	Description	Quantity
1	Micro controller PIC16F877A	1
2	330 Ω resistor	3
3	560 Ω resistor	1
4	2,2 kΩ resistor	1
5	4,7 kΩ resistor	
6	10 kΩ resistor	3
7	39 kΩ resistor	1
8	Electrolytic capacitor of 1μF and 50 V	2
9	Electrolytic capacitor of 1μF and 250 V	4
10	Capacitor of 15 pF	2
11	Microchip MAX 232	1
12	Crystal of 20 MHz	1
13	Digital temperature sensor DS18B20	1
14	LED	1
15	Optocoupler 4N25	1
16	LCD display of 16"x2"	1
17	Buttons	3
18	Female DB9 connector	1
19	10 kΩ potentiometer	1
20	Mosfet IRFZ48N	1
21	Schottky diode 1N5822	1
22	3A fuse	1
23	DC power source 5V 1A	1
24	DC power source 12V 3A	1

The electronic circuit for water heating control is presented in Fig.16. In this system, the optocoupler 4N25 was used to decouple control and power circuits. Consequently, the noise produced in one system will not be sent to the other. In addition, the Mosfet (IRFZ48N) is used to

provide the water pump switching at high frequency through the pulse width modulation (PWM). Because of the fast switching, a Schottky diode is inserted in parallel with the water pump power circuit in order to attenuate the reverse current produced during the motor shut down and to ensure an appropriate PWM signal. A digital temperature sensor DS18B20 with accuracy of 0.5°C (from -10°C to +85°C) were installed in the gas cooler to measure the water outlet temperature.

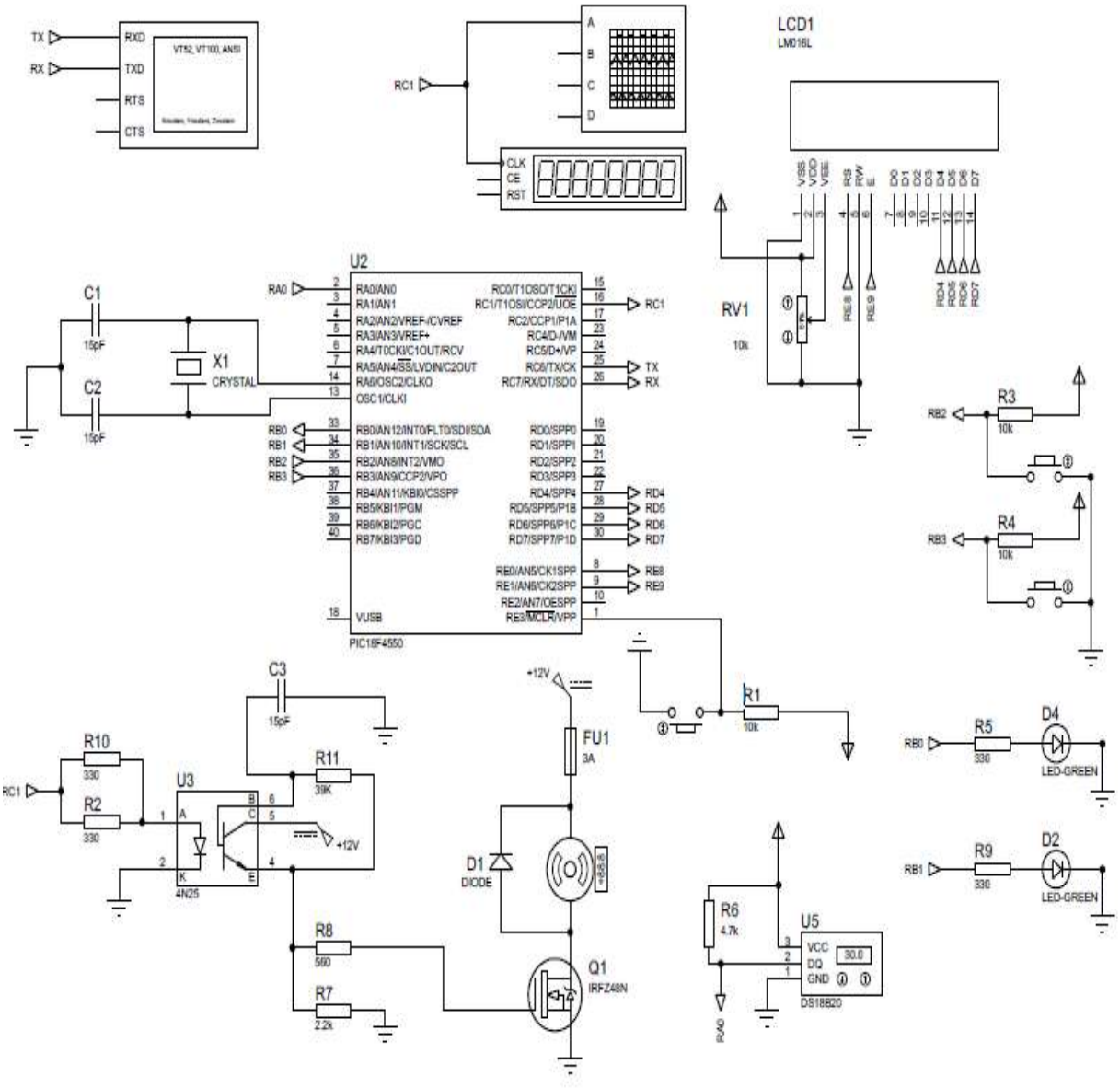

FIGURE 16 - Electronic circuit for water heating control.

4 METHODS

The heat pump used in this study was developed to produced hot water for bathing. Then, the first step of control in the system is the water heating, presented in section 4.1. As previously discussed, there is an optimum high pressure in the carbon dioxide system that lead the heat pump to operate with a maximum COP. The section 4.2 presents the methods related of the experimental evaluation of the specific internal area of the expansion device that leads the system operation near to the optimum high pressure and it need to occur with an adequate superheat. The sections 4.1 and 4.2 present a low-cost solution using a basic cycle configuration as presented in section 2.2.1. This proposal was considered a low-cost solution because of the basic cycle configuration as well as the use of the embedded system that is an economical alternative to provide control. The section 4.3 shows the methods to evaluate the effects of the solar radiation variation in the superheat by a distributed mathematical model. It brings up an advanced solution to control the superheat. However, to use this solution it is necessary a dual expansion device configuration as presented in in section 2.2.1.

4.1 Water heating control system

The Eq. (2) presents the heat transfer from the CO_2 in the gas cooler ($\dot{Q}_{GC}$). The $\dot{m}_{CO2}$ is CO_2 mass flow rate, h_i and h_o are CO_2 enthalpy in the inlet and outlet of the gas cooler, respectively. It could be considered that all energy of the CO_2 in the gas cooler is transferred to the water, as presented in Eq. (3). In Eq. (3) the water inlet and outlet temperature are represented by T_{wi} and T_{wo}, respectively. The specific heat of water at constant pressure is $c_{p,w}$ and $\dot{m}_w$ is the water mass flow rate.

$$\dot{Q}_{GC} = \dot{m}_{CO2}\left(h_i - h_o\right) \tag{2}$$

$$\dot{Q}_{GC} = \dot{m}_w c_{p,w}\left(T_{wo} - T_{wi}\right) \tag{3}$$

The technical regulation in Brazil provides that the water temperature for human consumption should not exceed 40ºC (ABNT, 1993, p.4). Shao *et al.* (2004) discussed that 45°C is the adequate water temperature for directed human consumption, without storage. On the other hand, if the water will be stored, the process of water heating should not allow the development of Legionella bacteria. Kim *et al.* (2002) presented chemical and thermal methods to prevent the proliferation of Legionella. Among the chemical methods, the chlorine is the most effective solution. For an

effective thermal control the water storage temperature must be equal or higher than 60°C (ASHRAE, 2000; BENSOUSSAN, 2014).

The water inlet temperature depends on the environmental conditions. Then, when the gas cooler heat transfer changes, the water mass flow rate needs to be modified for keeping the outlet water temperature at the appropriate value. The PID control adjusts the water outlet temperature. The goal of the control system is to keep the water outlet temperature in the correct set point (45°C to direct consume or 60°C to storage). For that purpose, the DC motor water pump receives a PWM (pulse width modulation) signal and modify the water mass flow rate in the gas cooler.

The control of the water outlet temperature will be realized in different conditions of the environment and CO_2 cycle. In that way, the identification and tuning of the control system is important for an adequate performance.

4.1.1 System identification and tuning process

The system identification aims to obtain the mathematical model able to describe the dynamic behavior of the system from the input signal (water mass flow rate) and the output (water outlet temperature). In accordance to the dynamics of the water heating system it was chosen a first-order plus dead time model and using the experimental data were obtained the static gain, the time constant and the dead time. After the model validation process a classic parallel PID control was chosen. According to Campos and Teixeira (2010) the PID controller is the most used in the industry for closed-loop system. The authors describe the advantages of PID control as good performance, versatile structure, low number of parameters to set or tune, and it is easy to associate parameters of setting and tuning. The Eq. (4) shows the implementation of classic parallel PID. The variable u is the controller output, t is the time, K_p is the proportional gain, e(t) is the error uring the time, T_I is the integration time and T_d is the derivative time.

$$u(t)=K_p\left(e(t)+\frac{1}{T_I}\int_0^t e(t)dt+T_d\frac{de(t)}{dt}\right) \quad (4)$$

Then, the tuning process was carried out. The tuning process presented the proportional, integrative and derivative gain and the quality scores showed the best tuning method for this water heating system. The system identification and tuning process used in this controller were presented by Fonseca (2018). For that purpose, an experiment was carried out in CO_2 DX-SAHP. The water volumetric flow rate was kept constant until the system reach the steady state and then, a new value

of the water volumetric flow rate was imposed by the water pump. After some minutes, the system achieved other steady state. During the experiment the water volumetric flow rate (entrance data) and water outlet temperature (output data) were measured. Then, the gain in the entrance and output variable were obtained.

4.1.2 Digital control

In an embedded system, only discrete signals can be implemented. So, approximations were used in the controller equation for integral and derivative terms. The derivative term was approximated by a differential equation using Euler method (Eq. (5)). The discrete version of the integral term was obtained using Tustin method (Eq. (6)). In this technique, the integral, or area, between two points is approximated by a rectangle. The base of the rectangle is the time, and the height is the average temperature between the current time and the previous instant of time. The Eq. (6) also considers the integral in the previous instant of time.

Therefore, the Eq. (4) is rewritten in the Eq. (7) and this equation can be implemented in an embedded system.

$$\frac{de(t)}{dt} \cong \frac{e(kT)-e(kT-T)}{T} \tag{5}$$

$$\int_0^{kT} e(t)dt \cong u(kT-T)+\frac{e(kT)-e(kT-T)}{2}T \tag{6}$$

$$u(t)=K_p e(t)+u(kT-T)+K_i\frac{e(kT)-e(kT-T)}{2}T+K_d\frac{e(kT)-e(kT-T)}{T} \tag{7}$$

In the Eq. (5), Eq. (6) and Eq. (7) K_i is the integral gain, K_d is the derivative gain, e(kT) is the current error, e(kT-T) is the error in the previous instant of time, u(kT) is the controller output in the current time and u(kT-T) is controller output in the previous instant of time.

The values used in this work are 4.37 for K_p, 0.18 for K_i and 6.51 for K_d.

4.1.3 Error evaluation

To evaluate the controller errors two methods were used: maximum absolute error (MAE), as shows Eq. (8) and root mean square error (RMSE) calculated by Eq. (9). Where $T_{ow,i}$ is the current

water temperature, $T_{ow,set}$ is the water temperature correct value (as described in subsection 4.1) and n is the number of points.

$$MAE = \max_i \left| T_{ow,i} - T_{ow,set} \right| \tag{8}$$

$$RMSE = \sqrt{\frac{\sum_{i=1}^{n} \left(T_{ow,i} - T_{ow,set} \right)^2}{n}} \tag{9}$$

4.1.4 Software flowchart

The software developed to control the water heating presents the following steps: first, the initial configurations were done, and after that, the temperature is obtained at the time defined by the microcontroller timer. With the current water temperature, its value is compared with the desired value (set point) and the error is calculated and sent to the PID function. The output of the PID function defines the duration of the duty cycle of the PWM signal. Then, the PWM signal is sent to water pump motor. Finally, the data is displayed on the LCD and sent by USB port to a computer. Figure 17 shows the software flowchart. The current version of the C program language for the control of the water heating system is presented in Appendix B.

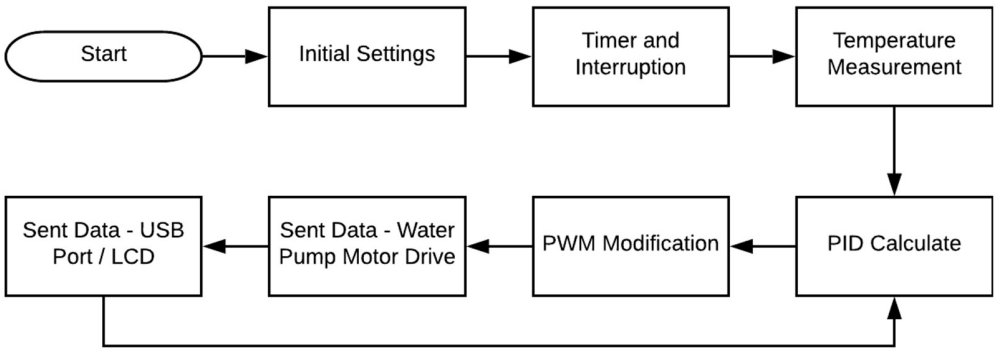

FIGURE 17 - Water heating control flowchart.

4.2 Evaluation of the expansion valve opening

The DX-SAHP is installed in Belo Horizonte, Brazil. The total amount of energy received by the solar evaporator is derived from convection, atmospheric air (latent heat) and solar radiation. In this work, the valve opening effect was evaluated considering Lower Solar Radiation (LSR) and Higher Solar Radiation (HSR), with a radiation flux average of 48W/m^2 and 715 W/m^2, respectively. These values are used as a reference to address each test. The total amount of energy

received in the evaporator is done by convection, latent heat and solar radiation. During the tests, the solar radiation presented stable values for both, HSR and LSR, like those illustrated in Fig.18. The expansion valve opening represents the ratio between the current number of turns and the maximum number of turns of this device, that is ten turns. In this study, it was investigated the interval from 0.1 to 0.4. Opening values superior to 0.4 make the DX-SAHP operates in a subcritical cycle, with a considerable decrease in the performance of the system.

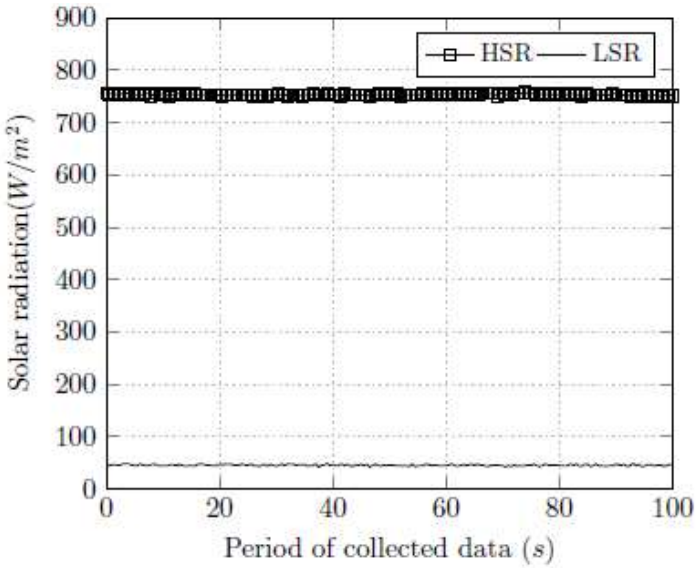

FIGURE 18 - The variation of solar radiation function of the period of collected data.

Table 5 presents the environmental conditions and their respective maximum relative deviation. As is shown in Tab. 5 the wind speed is characterized by light breezes, and for that condition this parameter does not have a significant effect on the performance of a DX-SAHP as reported by Kong *et al.* (2011).

TABLE 5 – Average environmental conditions and maximum relative deviation

Item	Ambient Temperature [°C]	Uncertainty Ambient Temperature	Relative Humidity	Uncertainty Relative Humidity	Wind Speed [m/s]	Uncertainty Wind Speed
LSR	24.95	± 1.76%	60.3%	± 3.80	2.17	± 1.38
HSR	25.53	± 3.17	57.0%	± 7.01	1.73	± 3.80

For all tests, the cold tap water entered in the gas cooler at 25°C and a PID kept the water outlet temperature constant at 60°C. In that way, the DC motor of the water pump received a PWM (pulse width modulation) signal and modified the water mass flow rate at the gas cooler inlet. The

set-point of the water at the gas cooler outlet was defined as 60°C to minimize the risk of Legionellosis bacteria formation in the water. The system operation occurred at this fixed temperature to reproduce a real operating condition. The measurements and data acquisition were performed just after the system reached the steady-state condition. As an example, Fig.19 shows the compressor pressures at the suction and discharge. First, the system is operating in the steady-state with an opening of 0.1, until the first dashed line. At this moment, the expansion valve opening was changed from 0.1 to 0.15. After reaching a new steady-state, the data for the opening turn of 0.15 was collected during the interval delimited by the second and third dashed lines. After the third dashed line, the valve opening was changed from 0.15 to 0.2. For the results presented in section 5.2, each point in a steady-state condition is an average of 200 data, gathered in a rate of two measurements per second, as solar radiation presented in Fig.18. The procedure to analyze the steady-state is applied for all variables and expansion valve openings.

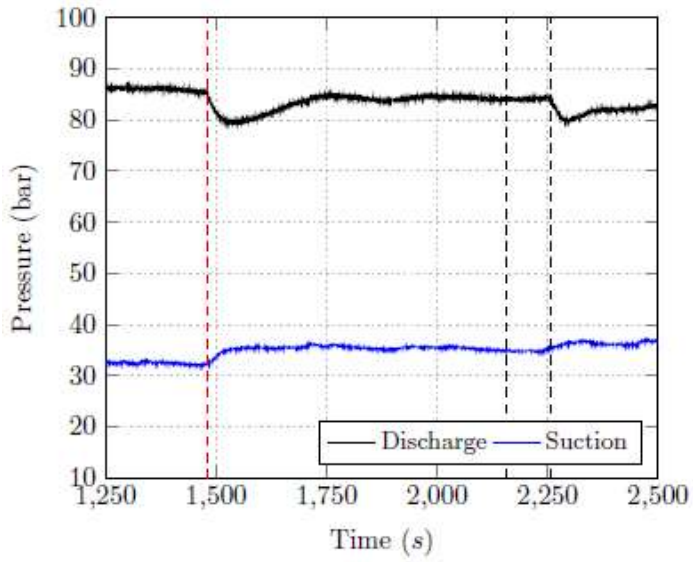

FIGURE 19 - Collected data in steady state.

4.3 Evaluation of the effects of the solar radiation variation in the superheat

4.3.1 Mathematical model

This section presents the DX-SAHP evaporator model to evaluate the effects of the solar radiation variation in the superheat. This model was developed and validated experimentally by Faria *et al.* (2016). The water, for residential usage, is heated in the gas cooler of the heat pump and stored in a well-insulated reservoir. The evaporator operation depends on others system

components, particularly the expansion device and compressor. Therefore, the evaporator model must be coupled with the models of these two components. The expansion device model provides the refrigerant mass flow rate and enthalpy at the evaporator inlet, while the compressor model supplies the refrigerant mass flow rate at the evaporator outlet. During the simulations, all variables of the gas cooler were considered constant. For the objectives of this part of the work, this assumption is appropriate because a small variation in the solar radiation causes slight changes in gas cooler operation, and only variations of 10% in the solar radiation were used to simulate the system dynamic behavior. However, in the results presented in the model validation section, the gas cooler parameters practiced in the experimental tests were also used in the mathematical model.

4.3.1.1 Expansion device model equations

A small needle valve is used to control the refrigerant expansion process. The fluid passes rapidly through this valve so that the process is practically adiabatic and isenthalpic in steady state. In consequence, the refrigerant enthalpy is given by Eq. (10). In addition, the refrigerant mass flow rate provided by the needle valve can be calculated by Eq. (11), as presented by Park *et al.* (2007).

$$h_{f3} = h_{f4} \tag{10}$$

$$\dot{m}_{f4} = C.A_{orf}\sqrt{2\rho_{f3}\left(P_{f3}-P_{f4}\right)} \tag{11}$$

In these equations, $\dot{m}$, h, ρ, and P represent the mass flow rate, enthalpy, density, and pressure, while the index *f* reports to the refrigerant and the number indexes *3* and *4* correspond to the inlet and outlet of the needle valve, respectively. The parameter *C* is the discharge coefficient and A_{orf} is the cross-section area of this valve.

4.3.1.2 Compressor model equations

The refrigerant compression process occurs in a reciprocating compressor. This component operates practically in steady state because the compressor has a small volume and its rotational speed is high. Thus, the mass flow rate imposed by the compressor is given by Eq. (12), as presented by Faires and Simmang (1983) and the volumetric efficiency of the compressor is calculated by Eq. (13).

$$\dot{m}_{fl} = N \rho_{fl} V \eta_v \tag{12}$$

$$\eta_v = 1.1636 - 0.2188\left(\frac{P_2}{P_1}\right) + 0.0163\left(\frac{P_2}{P_1}\right)^2 \tag{13}$$

In these equations, N is the speed rotation, η_V is the volumetric efficiency of the compressor and V the displacement. The index numbers *1* and 2 correspond to the inlet and the outlet of the compressor, respectively. And the isentropic efficiency is considered equal to 70%.

4.3.1.3 Evaporator model equations

The heat pump evaporator consists of a solar radiation absorber, on which a tubular coil is fixed. The refrigerant fluid flows inside of the tube, receiving energy in different ways: direct and diffuse solar radiation, exchange of heat by infrared between the absorber and its neighborhood, heat exchange by convection between ambient air and absorber, and condensation of water from the environment in the absorber.

The following considerations were assumed during the development of the evaporator mathematical model: (i) the liquid and vapor phases of CO_2 are in thermodynamic equilibrium in the boiling region; (ii) the heat transfer in the tube at the axial direction is negligible; (iii) the refrigerant flow is unidirectional; (iv) the physical properties of CO_2 and copper tube are uniform in each tube cross-section; (v) the contact resistance between the coil and the absorber is negligible; (vi) the tube wall resistance is negligible; (vii) all tube is considered straight. From these considerations, the balances of energy, mass, and momentum applied for the refrigerant in each coil section generate Equations 14, 15, 16A and 16B, while the balance of energy applied for the coil generates Equation 17. Appendix C shows the development of these equations.

$$\frac{\partial h_f}{\partial z} = \frac{1}{G_f}\left[\frac{\partial P_f}{\partial t} - \rho_f \frac{\partial h_f}{\partial t} + H_f \frac{p_f}{A_f}\left(T_w - T_f\right)\right] \tag{14}$$

$$\frac{\partial G_f}{\partial z} = -\frac{\partial \rho_f}{\partial t} \tag{15}$$

$$\frac{\partial \overline{P_f}}{\partial z} = -\frac{\partial G_f}{\partial t} - \left(\frac{dP}{dz}\right)_{fr} - g\rho_f \sin\left(\theta\right) \tag{16A}$$

$$\overline{P_f} = P_f + G_f^2 \left[\frac{x^2 v_v}{\alpha} + \frac{(1-x)^2 v_l}{1-\alpha} \right] \tag{16B}$$

$$\rho_w A_w c_{pw} \frac{\partial T_w}{\partial t} = \left[(W - D_0) F + D_0 \right] \left[S - U_L \left(T_w - T_{sky} \right) \right] - H_f A_f \left(\mathrm{T_w} - \mathrm{T_f} \right) \tag{17}$$

In these equations, in addition to the previously defined variables, there are the variables G, v, and T, which are the mass flux, specific volume, and temperature. The term $\overline{P_f}$ in the Equation (16A) is the refrigerant modified pressure, whose value is defined by Equation (16B). Still in the Equations (16A) and (16B), the terms g and θ are the gravitational acceleration and the angle of inclination of the solar absorber (evaporator) in relation to the horizontal, and the terms x and α are the quality and refrigerant void fraction. The indexes l and v refer to the liquid and vapor phase of the refrigerant, and the index w refers to the tube wall. The symbol $\partial/\partial t$ refers to the temporal derivate and $\partial/\partial z$ refers to the spatial derivatives in the direction of the flow. T_{sky} is the temperature of the sky, considered equal to the ambient air temperature.

In Eq. 14, A_f and p_f are the cross-section area and the perimeter internal of the tube. The correlations used to determine the coefficient H_{f} for the boiling region were those proposed by Cheng *et al.* (2006, 2008). For the superheating region, H_{f} is given by Dittus-Boelter, presented by Incropera and DeWitt (1999). In order to calculate the refrigerant void fraction in Eq. (16B), the correlation of Rouhani and Axelsson (1970) was used. In Eq. (16A), the pressure loss $(dP/dz)_{\mathrm{fr}}$ due to the friction in the boiling region is calculated by the correlation proposed by Friedel, and recommended by Cheng *et al.* (2008) as the one that produces the best results. In the superheat region, friction pressure loss is given by Fanning equation and the friction factor is determined by Blasius equation, described by Ozisik (1985).

In Eq. (17), ρ and c_p are the density and specific heat of the cooper (tube wall), W is the distance between two adjacent tubes (half the length of the fin), F is the fin efficiency, D_o is the outside diameter of the tube; A_w is the cross-section area of the tube wall. With regard to the combined coefficient $\mathrm{U_L}$, the natural convection part is obtained as proposed by Palyvos (2008), and the condensation part is determined as presented by Huhtiniemi and Corradini (1993). The equations used to obtain the direct and diffuse radiation and the heat exchange by infrared radiation are calculated according to the proposals of Duffie and Beckman (2013) and Kalogirou (2009). For more details on heat transfer, void fraction and pressure loss calculations, see Faria *et al.* (2016).

4.3.2 Discretization of the evaporator equations

Equations 14-17 form a system of four equations and four unknowns: the enthalpy, the pressure, the mass velocity of the refrigerant and the tube wall temperature. To solve this equation system, the implicit finite difference method was adopted with the evaporator tube divided into N control volumes and with the spatial and temporal derivatives approximated by Equations 18 and 19:

$$\frac{\partial y}{\partial z} = \frac{y_o - y_i}{\Delta z} \tag{18}$$

$$\frac{\partial y}{\partial t} = \frac{y - y^0}{\Delta t} \tag{19}$$

In these equations, the independent variables z and t are the position and time, and Δz and Δt are the position and time steps adopted in the numerical solution. The dependent variable y can be the temperature, pressure, enthalpy, density, mass flow rate, etc. In Eq. (18), the values y_o and y_i represent the variable at the analyzed control volume outlet and inlet at time t. In Eq. (19), y and y^0 correspond to the values at the control volume center at time t and $t-\Delta t$, respectively, which are approximated by the arithmetic average between the values of y at the control volume inlet and outlet.

4.3.3 Method of equations resolution

In order to calculate the model output variables at the first step of time, the refrigerant fluid and the tube wall temperature must be provided, as well as the refrigerant mass distribution along the tube (initial conditions). In order to accelerate the model resolution, Equations 14 to 16 (refrigerant) are solved separately from Equation 17 (tube). First, a spatial profile of the tube wall temperature and a pressure P_{f4} at the needle valve outlet are hypothetically assumed. These variables are model output, but guessed values are adopted initially and corrected later by trial and error. Then the mass velocity G_{f4} and the refrigerant enthalpy h_{f4} at the evaporator inlet are calculated by Equations 10 and 11, considering the following data (model input variables): refrigerant pressure and temperature at the needle valve inlet and pressure P_{f4}. With the values of G_{f4}, h_{f4} and P_{f4} (inputs of the first control volume), it is possible to calculate by Equations 14, 15 and 16 the corresponding values at the volume output, which, in turn, are used to supply the

calculations to the next control volume. This procedure is repeated throughout the entire boiling region, where specific correlations of heat transfer, pressure loss and void fraction are employed.

The tube position where is located the end of the boiling zone is determined when the enthalpy calculated at the volume outlet is equal to or slightly greater than the enthalpy of the saturated vapor (quality equal to 1). The superheat zone takes place from this position. The calculation procedure is basically the same as before, except that now the correlations used to calculate the heat transfer and pressure loss are for one-phase flow and the refrigerant density is calculated for pure vapor. With the refrigerant variables obtained at the evaporator end (output of the last control volume), it is possible to use Equation 12 to calculate the refrigerant mass flow rate $\dot{m}_{f1}$ imposed by the compressor. If this mass flow rate is not equal to the mass flow rate derived from Equation 15 at the evaporator outlet, the refrigerant pressure at the evaporator inlet (P_{f4}) should be corrected, and all the calculation procedure is repeated. After the second interaction, the Newton-Raphson algorithm is used to accelerate the convergence between the mass flow rates given by Equations 12 and 15 (within a defined error margin).

After solving the refrigerant fluid equations and obtaining its temperature profile, these data can be used in Equation 17 in order to find the temperature profile of the tube wall. This profile is then used to perform again all calculations involving the refrigerant equations. The overall calculations are repeated until there is stability in the wall temperature profile. The output variables can be updated as new initial conditions and the calculations for the next time instant can be done. In this new time, the boundary conditions must be also updated (for example, the solar radiation can increase or decrease in value). Figure 20 shows the mathematical model flowchart with all data and complete procedure of calculation.

To perform the simulations, the programming language used was Fortran. The computer was DELL model Inspiron 14 2640 and the processor was Intel Core i-5.

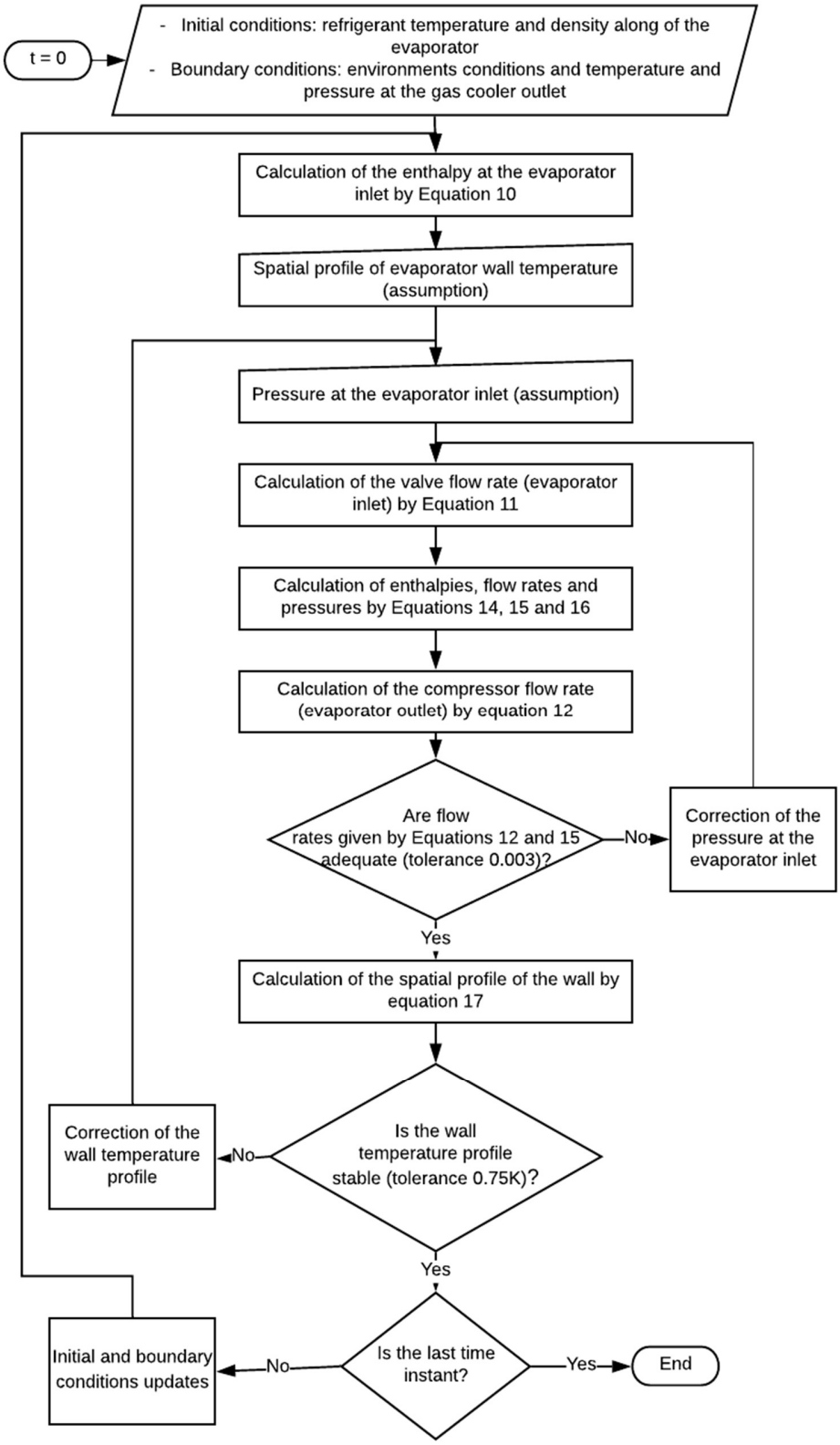

FIGURE 20 - Mathematical model flow chart.

5 RESULTS

This chapter presents the results obtained in this work and it is divided in three parts. First, the results related to the control system of the water temperature. Second, it is evaluated the expansion valve opening influence in the system. Finally, it is presented the effects of the solar radiation variation on the superheat using a distributed mathematical model.

5.1 Water heating control system

5.1.1 Effects of the variation of water volumetric flow rate

The first analysis related to the water heating control system was carried out to evaluate the effects of the variation of water volumetric flow rate. The goal of this experiment was to determine the water volumetric flow rate influence in the superheat and gas cooler outlet pressure. The experiment was carried out on May 07th, 2018. The DX-SAHP was in the laboratory and the expansion valve opening was fixed in two turns. The water volumetric flow rate was fixed in three different values. In the Tab. 6 is presented the water outlet temperature (T_{wo}), superheat (ΔTs), gas cooler outlet pressure (P_3) and temperature (T_3). The increase of the water volumetric flow rate results in a decrease of the water outlet temperature, as showed Eq. 3. In the same way, the gas cooler outlet pressure and temperature reduce. It occurs because the water is able to receives more energy from CO_2. Then, it shows that the control of the water outlet temperature influences the optimum high-pressure control. On the other hand, the superheat changes little due to the variation of the water volumetric flow rate. During the experiment, the evaporator/collector conditions were kept constant, because of that superheat changed little. In consequence, the water outlet temperature control did not affect the superheat control.

TABLE 6 – Effects of water volumetric flow rate variation

Item	Water volumetric flow rate (L/min)	T_{wo} [°C]	ΔTs [°C]	P_3 [bar]	T_3 [°C]
1	0.68	48.13	8.2	75.20	29.15
2	0.94	42.38	9.0	72.24	27.81
3	1.21	36.65	8.8	70.45	26.96

5.1.2 Control of water outlet temperature at 60°C

To evaluate the suitability of the control of water outlet temperature the first step was to establish the DX-SAHP refrigerant mass. After experimental tests, the mass was defined

empirically. This quantity of mass was considered during the identification and tuning process. Using 645 grams, Fig. 21 presents de Pressure-Enthalpy diagram for the system with 0.2 expansion valve opening. Then, the mass of 645 grams is the selected CO_2 mass. The experiment was performed on April 26, 2018 in a sunny day.

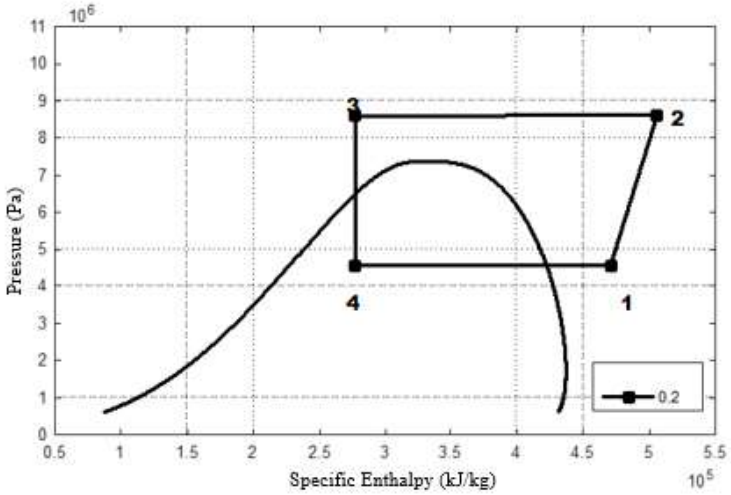

FIGURE 21 - Pressure-Enthalpy diagram, 0.2 expansion valve opening and 645 grams.

The DX-SAHP was put into operation at between 10:57 and 11:57 (HH:MM). During the experiment, the solar radiation flux increased slowly, as expected. It was 836 W/m² in average with a maximum and minimum value of 881 W/m² and 801 W/m², respectively. Figure 22 presents the variation of the water outlet temperature and voltage in water pump motor. The PID control was used to keep the water outlet temperature at 60°C. The back full line presents the water outlet temperature and the blue full line shows the voltage in water pump motor. Different opening area at the expansion valve and at the return lubricating oil to the compressor were used to check the adequacy of the controller. In that way, three different expansion valve opening (0.3, 0.4, 0.5) were used. The dashed black lines show for each period of time in which that expansion valve opening was used. Furthermore, during the experiment the lubricating oil returned twice to the compressor trough the opening of the oil return valve installed next to the oil separator. The dashed red lines show the instant of opening the oil return valve. In these cases, the valve was closed around 30 seconds after opening.

When the compressor is turned on, the water outlet temperature is 37°C. This high temperature occurs due to the non-return of the gas cooler to environment temperature after the last operation. However, Fig. 22 presents only temperatures above 54°C, due to the chosen scale. It can be noticed

that during the variation of expansion valve opening the controller is able to modify the water mass flow rate and keep the correct water outlet temperature. On the other hand, during the return of the oil to the compressor the controller is not able to keep the correct water outlet temperature as shows Fig. 22. In that case, the opening of the oil return valve results in the connection between the discharge and suction of the compressor. Immediately, the water outlet temperature decreases. In consequence, the water mass flow rate reduces until the minimum value. The minimum mass flow rate is defined from the minimum voltage that can be applied to the water pump motor and still allows the circulation of water in the gas cooler. However, this value is not enough to keep the water outlet temperature set point. Then, it decreases until the oil return valve is closed. Furthermore, it is possible to notice the same behavior for water outlet temperature (control variable input) and for voltage in water pump motor (control variable output).

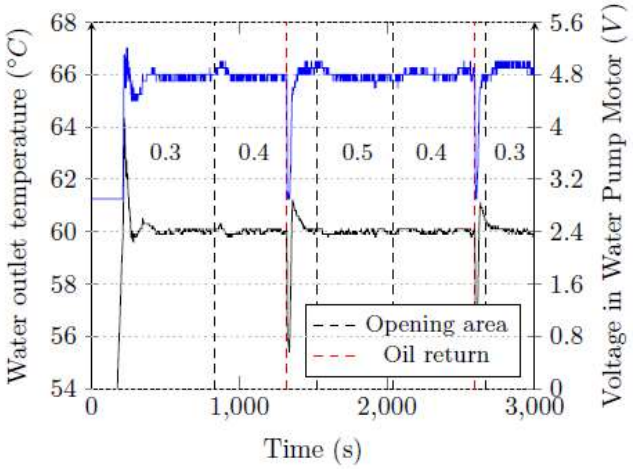

FIGURE 22 – Control of water outlet temperature at 60°C with 645 grams of CO_2 in the DX-SAHP.

The results show that system overshot is 4.3°C above the correct value. It is acceptable in this type of the system because it will operate for some hours to produce the appropriate amount of hot water. In addition, the RMSE and MAE are 0.606 and 4.6, respectively.

Another experiment was carried out on April 24th, 2018 in a cloud day. For that, the quantity of mass in CO_2 DX-SAHP was 620 grams, almost the same of the previously presented experiment. The average of the solar radiation was 600 W/m² and the maximum and the minimum value were 955 W/m² and 218 W/m², respectively. Figure 23 shows the solar radiation variation and the water outlet temperature. Furthermore, two different expansion valve opening were used, 0.2 and 0.3. The dashed black line shows for each period of time which expansion valve opening is used. The results show that the controller is able to control the water mass flow rate and keep

the correct set point despite the large variation of solar radiation and the change in the expansion valve opening. For this experiment, the RMSE and MAE are 0.141 and 0.4, respectively.

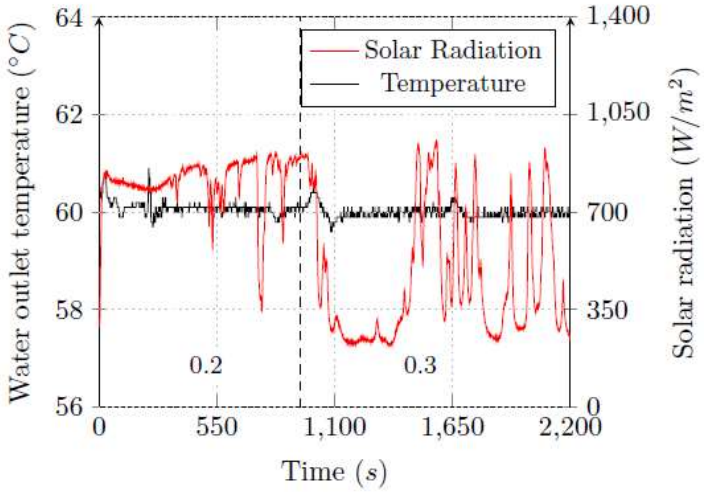

FIGURE 23 - Control of water outlet temperature at 60°C with 620 grams of CO_2 in the DX-SAHP.

An additional experiment was carried out on April 12th, 2018 in a cloud day with a solar radiation average of 138 W/m². For that experiment, the quantity of mass inside the equipment was 420 grams and the opening area was kept fixed in 0.5 turn. Figure 24 shows the variation of the volumetric flow rate and the water outlet temperature. It seems that the water outlet temperature was not kept in the correct set point and the volumetric flow rate changes during the experiment.

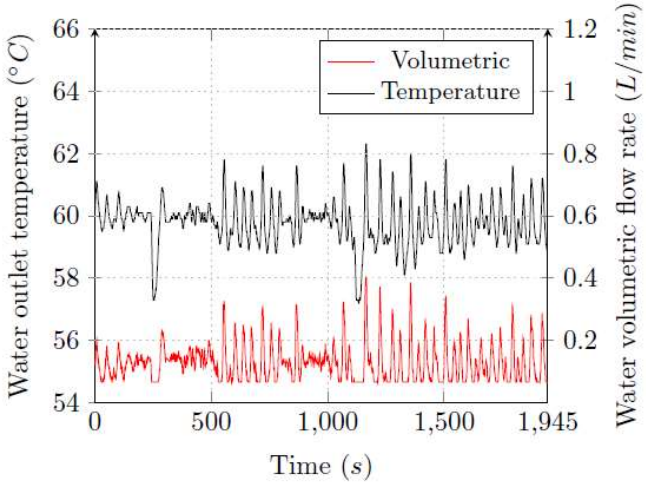

FIGURE 24 - Control of water outlet temperature at 60°C with 420 grams of CO_2 in the DX-SAHP.

The different system dynamic due to the different mass in the system could explain the variation of the water outlet temperature. Furthermore, along the experiment in different times the

volumetric flow rate was in the minimum value. In these cases, the controller is saturated at the minimum value in which the water pump can work. For this experiment, the RMSE and MAE are 0.774 and 2.8, respectively.

5.1.3 Control of water outlet temperature at 60°C and solar radiation step

In this sub-section, it was performed an experimental test to verify the effect of solar radiation step in the outlet temperature. Firstly, the heat pump was exposed to solar radiation of 767 W/m². The needle valve was opened, and the opening area was kept fixed in two turns. The system was turned on (compressor and water pump) and, after reaching the first steady state, the evaporator was covered with a stall, as presented Fig. 25, which reduced the solar radiation to 80 W/m². Approximately 20 minutes later, the DX-SAHP reached the second steady state. Finally, the stall was removed, and the solar radiation increased to 797 W/m² (value 4% higher than solar radiation for the first state). Again, after 20 minutes, the DX-SAHP reached the third steady state, which was close to the first steady state. Throughout the test, the ambient temperature and the relative humidity were 26°C and 50%, respectively; the water inlet temperature in the gas cooler was set at 25.8°C. CO_2 mass in the DX-SAHP was of 645 grams. The experiment was carried out on May 3rd, 2018.

FIGURE 25 - Solar radiation step experiment.

Figure 26 shows the solar radiation and water outlet temperature during the experiment. The PID controller was used to keep the water outlet temperature at 60°C. It can be observed that the water outlet temperature is almost constant during the experiment presenting a MAE equal to 0.3 and an RMSE equal to 0.081.

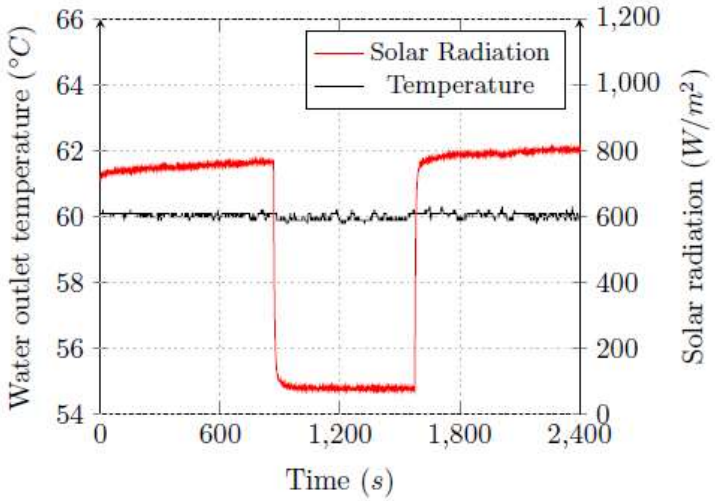

FIGURE 26 - Solar radiation step and water outlet temperature control.

Table 7 presents other effects of solar radiation step. First, the increase of the energy input in the evaporator/collector in high solar radiation results in a rise of CO_2 mass flow rate and consequently in water volumetric flow rate. CO_2 mass flow rate rise due to the increase of the compressor volumetric efficiency and expansion valve discharge coefficient as will be discussed in subsection 5.3.2. Also, the rise of the CO_2 mass flow rate results in COP increases. The mass flow rate was determined with an average uncertainty of 0.58 kg/h and the COP was calculated with an average uncertainty of 0.07.

TABLE 7 – Effects of solar radiation step

Solar radiation [W/m²]	Water volumetric flow rate (L/min)	CO_2 mass flow rate (kg/s)	P_1 [bar]	P_3 [bar]	T_2 [°C]	T_3 [°C]	ΔTs [°C]	COP
766.66	0.71	0.0082	47.61	82.03	89.23	32.77	11.95	2.57
79.52	0.59	0.0075	43.15	82.11	81.71	33.72	5.08	2.15
796.96	0.73	0.0083	47.61	82.42	89.09	33.16	12.51	2.53

Figure 27 presents the pressure-enthalpy diagram for two different solar radiations, 766.66W/m² (HR) and 79.52 W/m² (LR). The increase of the suction pressure of the compressor (P_1) due to the rise of solar radiation is presented in Tab. 7 and also in Fig. 27. On the other hand, the gas cooler outlet pressure and temperature remain almost constant during the solar radiation

step. It seems that these variables are mostly influenced by the water mass flow rate as discussed in subsection 5.1.1 and by the expansion valve opening area as will be presented in subsection 5.2.1. Finally, in low solar radiation the compressor outlet temperature decreases. It occurs because of the compressor inlet temperature decreases.

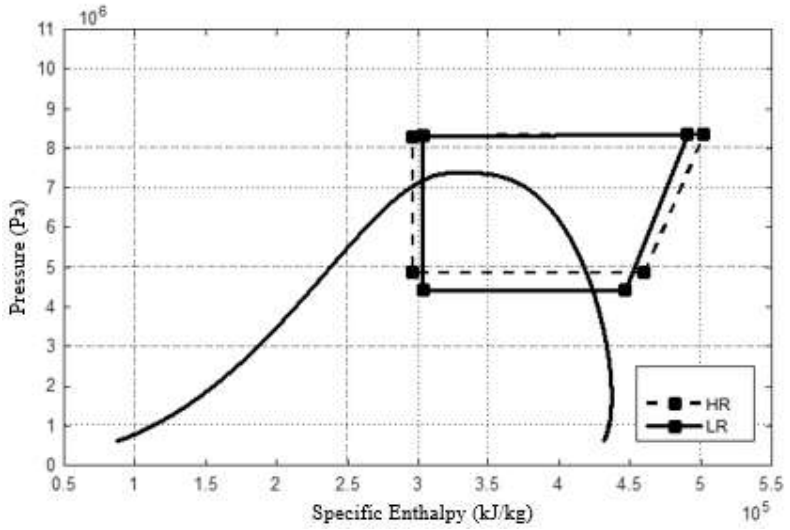

FIGURE 27 – CO_2 DX-SAHP pressure-enthalpy diagram for two different solar radiations

5.1.4 Control of water outlet temperature at 45°C

The last subsection of the water outlet temperature control was developed to analyze the direct consumption of hot water. Then, in that case, it considers 45°C with the correct set point of the water outlet temperature. The PID controller constants considered were not changed.

The first experiment was carried out on May 03rd, 2018 on a sunny day. In this experiment, the mass in the DX-SAHP was 645 grams. Figure 28 shows the solar radiation and the water outlet temperature during the experiments. The expansion valve opening was 0.5. The dashed red line shows the instant of the oil return valve opening. In this case, the valve was closed 15 seconds after opening. The study of the results shows that the system overshot is 4.4°C above the correct value. Also, the RMSE and MAE are 0.988 and 4.4, respectively. In general, the controller could keep the water outlet temperature in the correct set point.

Another experiment was carried out on April 24th, 2018 on a cloudy day. In this experiment, the refrigerant mass in the DX-SAHP was of 620 grams. Figure 29 shows the solar radiation and the water outlet temperature during the experiments. The expansion valve opening areas used were

0.4 and 0.3. The dashed black line shows the instant of change from one to another. The average of the solar radiation was 234 W/m², and the maximum and the minimum value were 755 W/m² and 141 W/m², respectively. The analyze of the results shows that the system overshot is 3.0°C above the correct value. Also, the RMSE and MAE are 0.429 and 3.0, respectively. In general, the controller could keep the water outlet temperature in the correct set point.

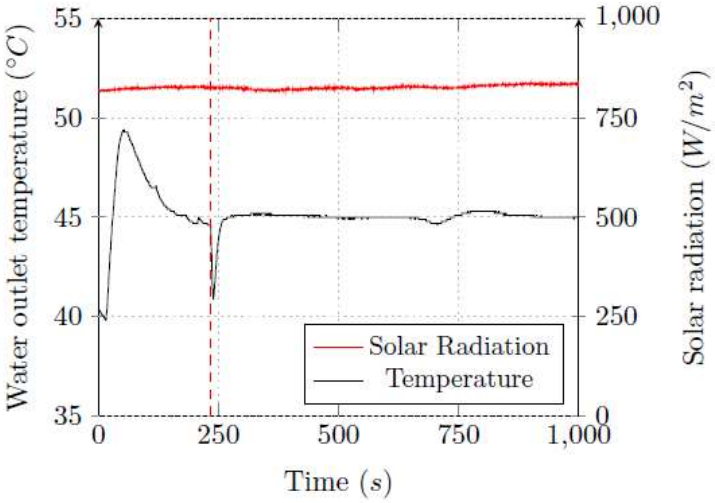

FIGURE 28 - Control of water outlet temperature at 45°C with 645 grams of CO_2 in the DX-SAHP.

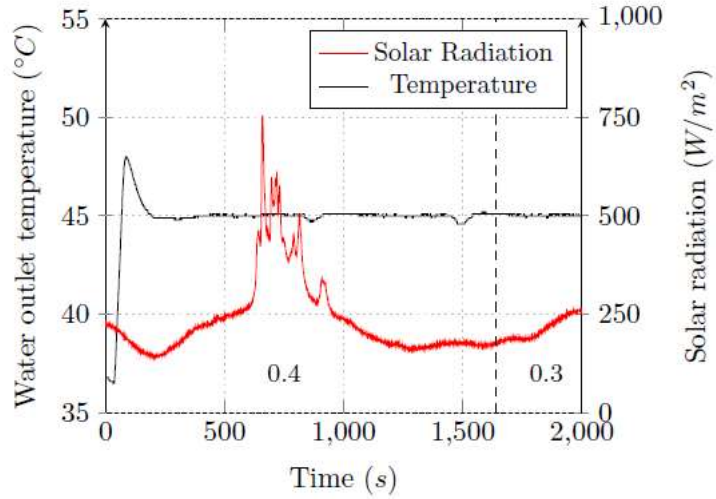

FIGURE 29 - Control of water outlet temperature at 45°C with 620 grams of CO_2 in the DX-SAHP.

5.2 Evaluation of the expansion valve opening

The experimental tests to evaluate the expansion valve opening were carried out on May 17th, June 05th and 12th, 2018. The following subsection presents the results and the discussions about them.

5.2.1 Pressure

The effect of the expansion valve opening on the diagram pressure-enthalpy is shown in Fig.30 for the HSR. The system high pressure reduced and the low-pressure increased as the expansion valve was opened. The same behavior was observed for LSR. The suction and discharge pressures for an opening turn of 0.1, were 32.73 bar and 86.16 bar, while for an opening turn of 0.4 were 49.20 bar and 76.69 bar, respectively. A similar effect on the gas cooler and evaporating pressures was previously presented by Wang *et al.* (2013). As the area increased due to the expansion valve opening, CO_2 mass tends to reduce in the gas cooler and increase in the evaporator. In that way, since the volume is the same, the density increased in the evaporator causing a rise in the evaporating pressure. On the other hand, the density was reduced in the gas cooler causing a reduction on its pressure.

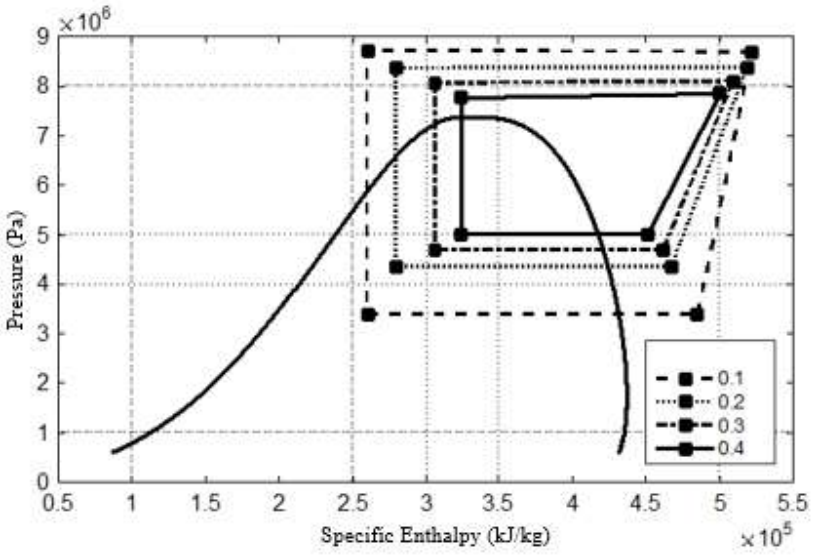

FIGURE 30 - The Expansion valve opening effect on the diagram pressure-enthalpy

Figure 31 illustrates the effect of the pressure for both cases, LSR and HSR. As expected, the gas cooler outlet pressure of the DX-SAHP has a very similar behavior in both instances analyzed, since the water inlet and outlet conditions at the gas cooler were maintained constant - 25°C and 60°C, respectively. The results also show that the variation in solar radiation has a slight influence on the gas cooler outlet pressure. Unlike in the gas cooler, the solar evaporator conditions were changed in the present test. Higher solar radiation resulted in a greater heat transfer in the evaporator, which leads to a higher inlet pressure in the compressor.

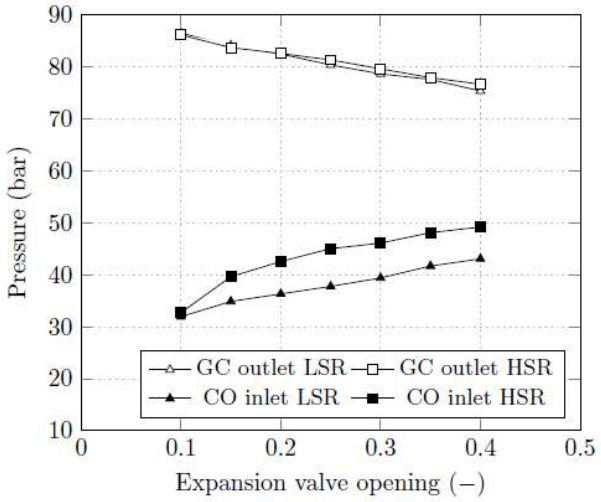

FIGURE 31 - Variation of pressure regarding the expansion valve opening

As shown in Fig.32, the compressor pressure ratio decreases for both cases (LSR and HSR) with the increase of the expansion valve opening. As expected, the compressor pressure ratio for HSR was lower than for the LSR because of the effect of the solar radiation in the evaporating pressure.

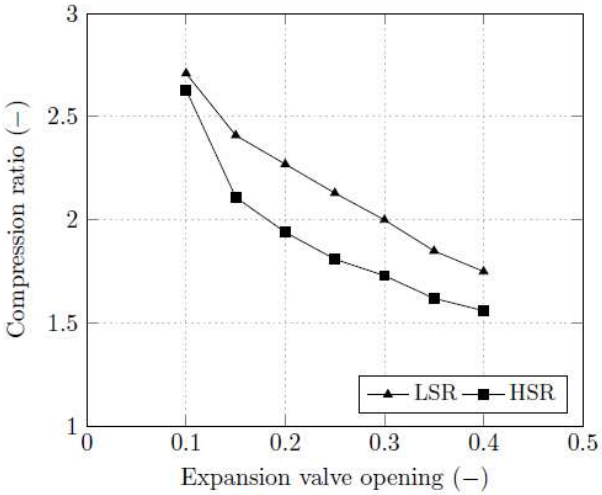

FIGURE 32 - Variation of compression ratio regarding the expansion valve opening.

5.2.2 Temperature

Figure 33 presents the temperature variation, caused by the increase in the expansion valve opening. Since the operating conditions for the water were the same for both cases analyzed (LSR and HSR), the outlet temperature in the gas cooler presented practically the same values to all

valve-opening. The slight augments in this temperature (from 25°C to 33°C) with the increase in the expansion valve opening, can be attributed to the rise in CO_2 mass flow rate.

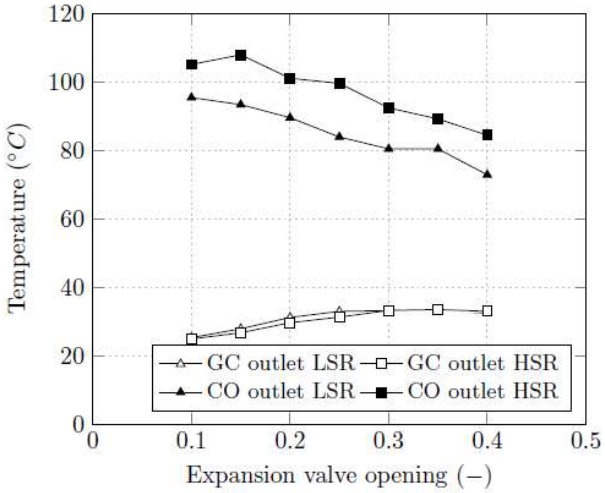

FIGURE 33 - Variation of temperature regarding the expansion valve opening

Moreover, it also can be observed the same behavior for the compressor outlet temperature, which decreases with the expansion valve opening for both conditions. The mass flow rate increased due to the augment in the expansion valve opening that resulted in a lower compressor outlet temperature. This trend of the compressor outlet temperature is also presented in Fig.30.

Furthermore, the values of the compressor outlet temperature for the HSR is more significant than the LSR. This effect occurred because of the increase in the useful energy in the evaporator, which causes an increase in the low pressure and the superheat. It leads to an increase in the temperature at the outlet of the compressor.

5.2.3 Carbon dioxide mass flow rate

Figure 34 presents the variation of CO_2 mass flow rate regarding the expansion valve opening. As expected, the opening of the expansion device produces an increase in CO_2 mass flow rate, as shown in Eq.11. Similar results can be found in the literature (LIU, CHANGHAI *et al.*, 2016; LIU, CICHONG *et al.*, 2018) for a CO_2 non-solar assisted system.

For the same internal area of the expansion device, the increase in solar radiation resulted in an augment in the mass flow rate. The same behavior was observed in work presented by Kong et al. (KONG; JIANG; *et al.*, 2018) for a R-134a DX-SAHP. Comparing the results in Fig.34 for LSR and HSR through the Eq.11, it is possible to notice this behavior. For the same internal area

of the expansion device, the fluid pressure, and density at the inlet of the expansion valve are the same, as previously discussed. The outlet pressure of the expansion valve increased contributing to decreasing the mass flow rate. Then, the increase in the mass flow rate was mainly due to the augment in the discharge coefficient. The two works presented in the previous paragraph (LIU, CHANGHAI *et al.*, 2016; LIU, CICHONG *et al.*, 2018) also showed the variation of the discharge coefficient due to others factors besides the internal area of the expansion device in CO_2 systems. However, in none of them, the analysis was made for a DX-SAHP.

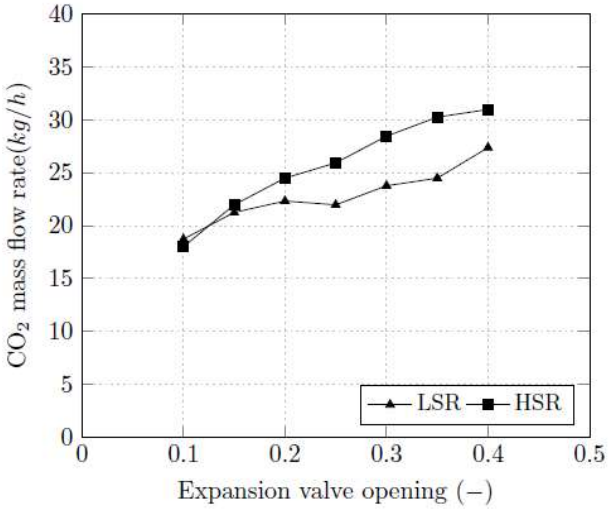

FIGURE 34 - Variation of mass flow rate regarding the expansion valve opening

For the expansion valve opening of 0.1, the mass flow rate for LSR was the same as HSR. It occurs because in that operating point, for both solar radiations, the low pressure is the same, as presented in Fig.31.

The mass flow rate can be also calculated by Eq.12 and the compressor volumetric efficiency can be obtained by Eq.13. Then, as described in Eq.13, the compressor volumetric efficiency increases in high solar radiation due to the reduction of compression ratio. Furthermore, the refrigerant density at the compressor inlet also increases for high solar radiation. The volumetric displacement and rotating speed do not change due to the solar radiation variation. Then, these factors contribute to increasing the mass flow rate. Furthermore, the mass flow rate was determined with an average uncertainty of 1.25 kg/h in this experiment.

5.2.4 Compressor power

The variation of the power consumption of the compressor due to the expansion valve opening is shown in Fig.35. The increase in solar radiation produced an increase in the mass flow rate and a decrease in the compression ratio, as previously discussed. As presented in Eq.20, an increase in the mass flow rate produced an increase in the power consumption of the compressor. On the other hand, the compressor enthalpy difference and the compressor thermal efficiency change during the process. Then, the power consumption of the compressor remains almost constant. Kong et al. (KONG; JIANG; *et al.*, 2018) presented the same behavior for a R-134a DX-SAHP.

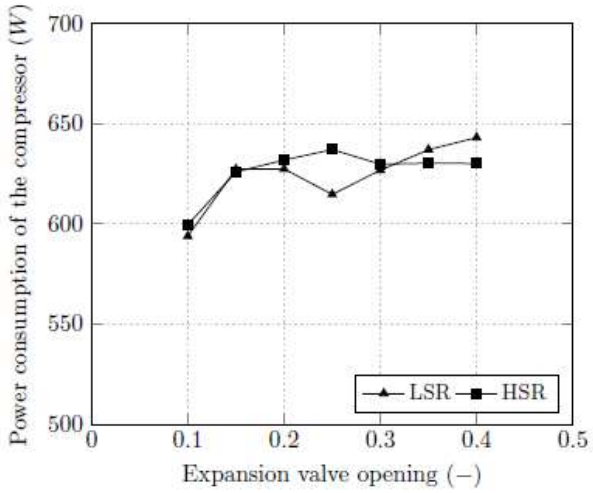

FIGURE 35 - Variation of power consumption regarding the expansion valve opening

$$\dot{W}_{co} = \frac{\dot{m}_{CO}\left(h_2 - h_1\right)}{\eta} \tag{20}$$

5.2.5 Heat transfer in the evaporator and the gas cooler

As shown in Fig.36, when the solar radiation increased, the heat transfer in the evaporator and gas cooler also increased. Two factors produce these augments, first the rise of energy in the evaporator results in a rise of CO_2 mass flow rate as presented Fig.34. Second, the difference of enthalpy in the evaporator and gas cooler increased when solar radiation increased as showed Fig.37.

Moreover, for the same solar radiation, CO_2 mass flow rate increased due to the opening of the expansion valve. The difference of enthalpy for the gas cooler and evaporator (Fig.37)

decreased in both solar radiations. Then, the heat transfer in evaporator and gas cooler is the product between CO_2 mass flow rate and the difference of enthalpy, which leads to a maximum heat transfer.

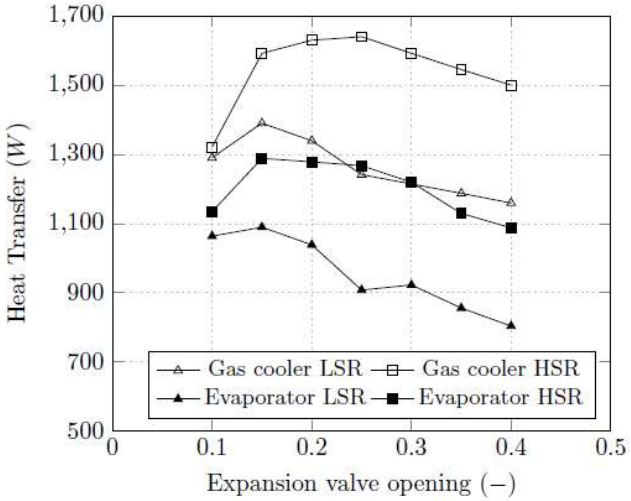

FIGURE 36 - Variation of heat transfer regarding the expansion valve opening

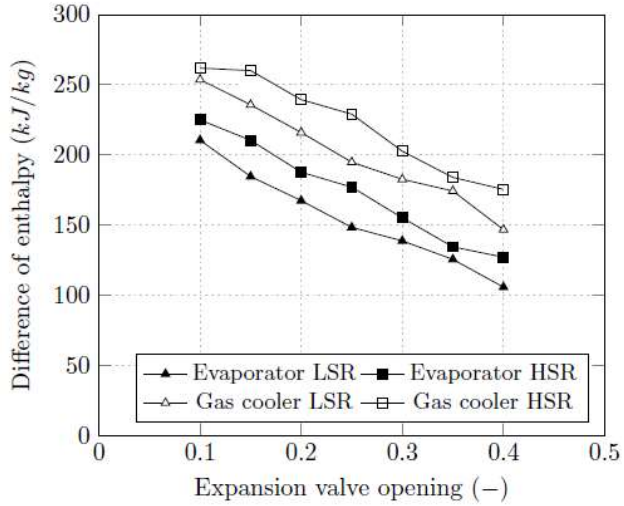

FIGURE 37 - Difference of enthalpy in the evaporator and the gas cooler regarding the expansion valve opening

5.2.6 Coefficient of performance

The measured COP of the system is presented in Fig.38. It can be noticed that the augment of solar radiation results in a COP increase. The observed trends are consistent with those earlier reported by Kong et al. (2011) for R22, Kong et al. (2017) for R410A and Mohamed, Riffat and Omer (2017) for R407C. As shown Fig.36, when the solar radiation increased, the heat transfer in

the gas cooler augmented. Also, the power consumption of the compressor is almost the same for both solar radiations analyzed. As the COP is calculated by Eq.21, it can be inferred that the COP increased due to the rise of heat transfer in the gas cooler.

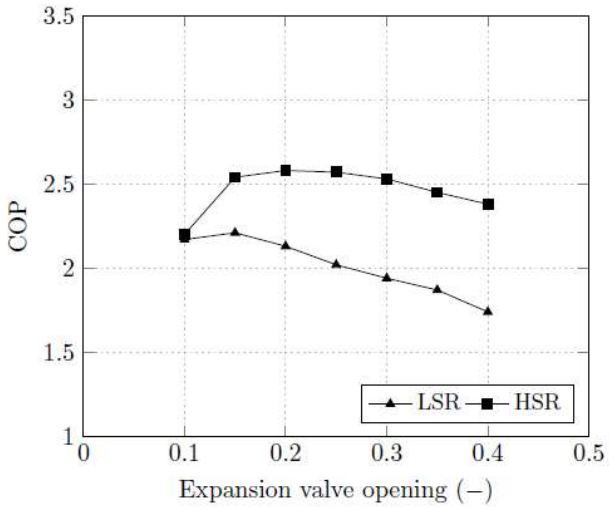

FIGURE 38 - Variation of COP regarding the expansion valve opening

$$COP = \frac{\dot{Q}_{GC}}{\dot{W}_{CO}} \tag{21}$$

Furthermore, there is an optimum COP for each solar radiation. Similar behavior for the optimum COP in a CO_2 system was previously reported in the literature for non-solar assisted heat pump (HOU; MA; *et al.*, 2014). Besides, the value of the expansion device opening that leads the system to the maximum COP was close regardless of solar radiation. Then, for a small CO_2 DX-SAHP, using a basic cycle as a configuration, a static expansion device as a capillary tube or manual valve could be suitable. In that way, it can reduce the cost of the equipment maintaining the performance in acceptable values. Also, it is important to highlight that for an opening area about of 0.2, the superheat is higher than 8°C for any solar radiation analyzed. This superheat can ensure the compressor integrity. Furthermore, the COP was calculated with an average uncertainty of 0.13 in this experiment.

5.2.7 Superheat analyze

After the results that presented the opening area of 0.2 as adequate, another experiment was performed on September 05, 2018. The opening area was fixed in 0.2. The experiment was carried out between 09:40 and 15:35 (HH:MM). Figure 39 presents superheat and solar radiation during

the experiment. It can be noticed that the solar radiation increases at a maximum value around midday and after that decreases, as expected. The rise of solar radiation produced an augment of heat transfer in the evaporator/collector. If the evaporator/collector has the same quantity of mass, the increase of the energy input resulted in a rise of the superheat. On the other hand, the decrease of solar radiation resulted in a superheat decrease.

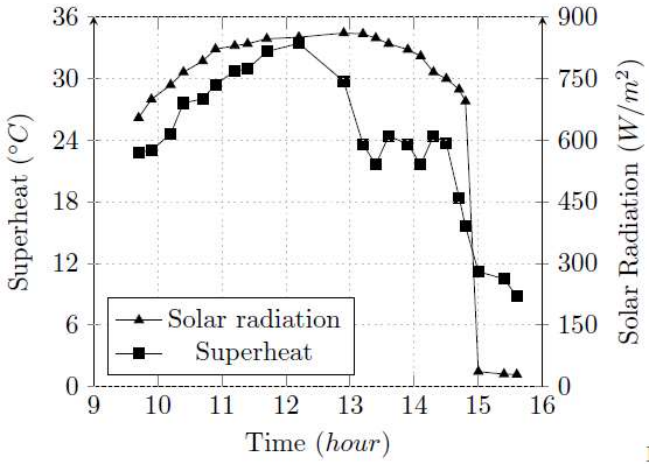

FIGURE 39 - Variation of superheat regarding the solar radiation

Figure 40 shows the COP and solar radiation during the experiment. As presented in Fig. 38, when the solar radiation was higher the COP was also higher. During the experiment the COP average was 2.33, the minimum value was 1.87 (at 15:35) and the maximum value was 2.69 (at 12:10). Using Figures 39 and 40 it can be noticed that the opening area of 0.2 led the DX-SAHP to operate with an acceptable performance and ensures safe superheat. In this case, it is still important include in the system a thermostat in the compressor discharge to limit the maximum temperature and ensure safe operation of the compressor in high solar radiations.

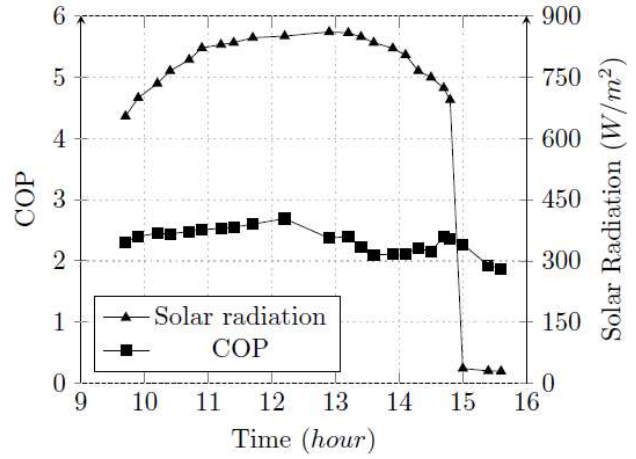

FIGURE 40 - Variation of COP regarding the Solar Radiation

5.3 Evaluation of the effects of the solar radiation variation in the superheat

The subsections 5.1 and 5.2 are useful to demonstrate that only the water outlet temperature control and the static expansion device are enough to ensure the adequate operation in a small size low cost CO_2 DX-SAHP, using a basic cycle configuration. However, in current section will be presented an advanced solution. It improves the performance of the system and it could be used in a dual expansion device configuration.

5.3.1 Model validation

The model validation is the process to evaluate whether or not the mathematical model can be used to predict, with some tolerance, the physical parameter of interest. After being approved in the validation procedure, the mathematical model is ready to be used in place of experimental tests, to simulate different scenarios and operating conditions, and produce reliable output data. The main advantage of the use of a mathematical model is the fact that it can be used to simulate conditions that may be difficult to assess through experimental tests. Additionally, the costs comprised in the simulations are generally smaller than that involved in the experimental tests, and the results are mostly generated in a shorter time.

The experimental procedure used for model validation was previously described in subsection 5.1.3.

Figure 41 shows the experimental results of the solar radiation (model input) and CO_2 evaporating temperature and the superheat in the DX-SAHP evaporator (model output), as well as the results generated by the model for these model output variables. It can be noticed that the decrease in the solar radiation produced an almost immediate reduction in the evaporating temperature and in the superheat. The reductions observed was due to the lower energy input in the DX-SAHP evaporator. In addition, a more accentuated and faster reduction was observed in the superheat than in the evaporating temperature. In other words, the gain of the superheat is higher, while its time constant is smaller compared to the values for the evaporating temperature. A similar behavior can be noticed when the solar radiation was increased, it resulted in an almost immediate rise in the evaporating temperature and in the superheat.

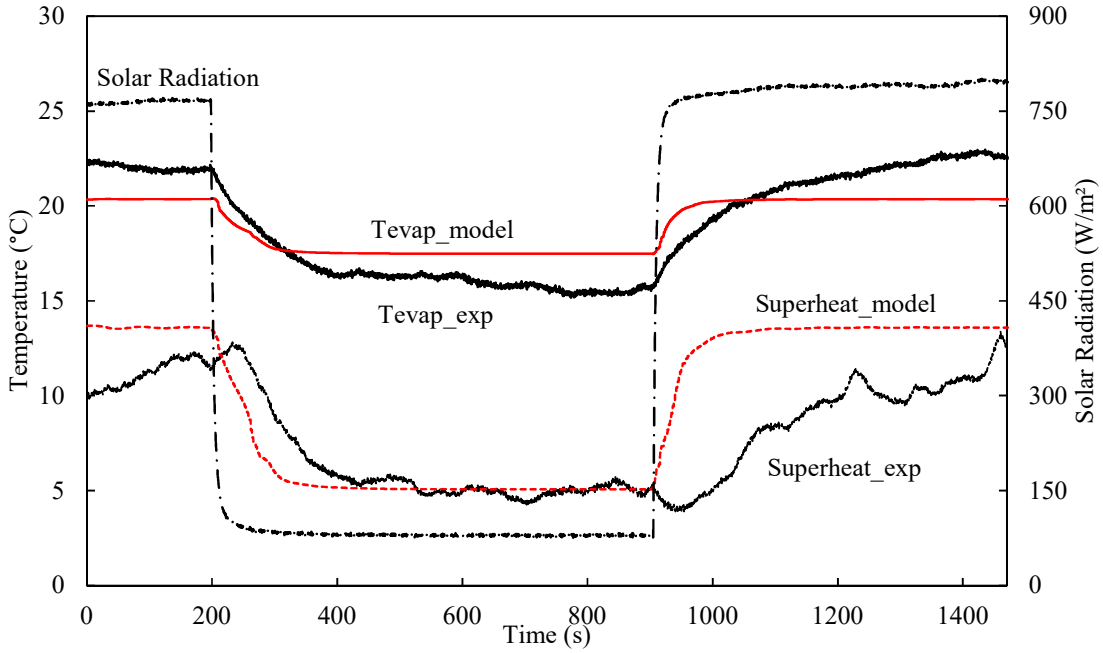

FIGURE 41 - Model Validation - effects of the solar radiation on the evaporating temperature and the superheat.

Figure 41 shows that the evaporating temperature and the superheat in the steady state obtained from simulations were close to the experimental results. When the solar radiation was equal to 80 W/m², the values of the superheat were 4.8°C (experimental) and 5.0°C (mathematical model). Furthermore, for this value of solar radiation, the values of the evaporating temperature were 16.2°C (experimental) and 17.5°C (mathematical model). It is important to highlight that the thermocouples used in this work presented an uncertainty of ±1°C.In addition, it can be noted that the dynamics of the mathematical model due to the variation of the solar radiation was faster than the dynamics of the experimental results. However, both lead the system to the almost same steady state value. An aspect that could explain the difference between the dynamics of the mathematical model and experimental data is the discharge coefficient C (presented in Equation 11) of the needle valve. To simulate the behavior of this valve, the equation provided by the manufacturer, that predicts C as a function only of the valve opening area was used. However, there are works that show the influence of other parameters in the factor C (HOU; LIU; *et al.*, 2014; PARK *et al.*, 2007).

5.3.2 Simulations results

Knowing how the evaporator of DX-SAHP responds to a sudden change in solar radiation is important because large and rapid deviations from the superheat set point for a long time may have extreme and negative effects on the evaporator itself and on other components of the heat pump. Studying the dynamical behavior of the assembly formed by evaporator, expansion device and compressor can provide valuable information on the system stability, as well as the ability to reach a new stationary steady state when the evaporator experiences an abrupt external disturbance.

A typical technique employed in the control theory to study dynamical systems, such as the direct expansion evaporator of this work, is called step response, which consists in obtaining the temporal evolutions of the outputs variables when a specific input variable changes from a value to another. In general, this technique requires several experimental tests. In the case of a direct expansion solar assisted evaporator, such tests can be expensive and difficult to perform. The use of a mathematical model, capable of reliably reproduce the temporal evolutions of the output variables when an input variable is changed abruptly, is a reasonable alternative.

The evaporator model was run with 2000 control volumes and a time step of two seconds. Values of temperature and mass flow rate previously obtained were used as initial conditions to simulate the superheat step response of the DX-SAHP evaporator to a sudden change in solar radiation. The evaporator was operating in the steady state (in the instant of the time of 150 seconds) with an evaporating temperature of 14.5°C, a superheat of 6°C and a mass flow rate of 30 kg/h when in a certain moment (t = 160 s in Figures 42 and 43, Radiation step 1), the solar radiation was reduced by 10%. As a result, the refrigerant temperature and pressure decreased. As provided by Equations 11, the mass flow rate in the expansion device increased, as shown in Fig. 42. In consequence, the refrigerant flooded the evaporator, and the superheat decreased, as showed in Figures 42 and 43. On the other hand, the mass flow imposed by the compressor, given by Eq. 12, tends to remain the same value because it depends basically of the refrigerant density at the compressor inlet, which values are 141.0 kg/m³ (at time of 160 s - Radiation step 1) and 141.1 kg/m³ (at time of 170 s - Valve step 1).

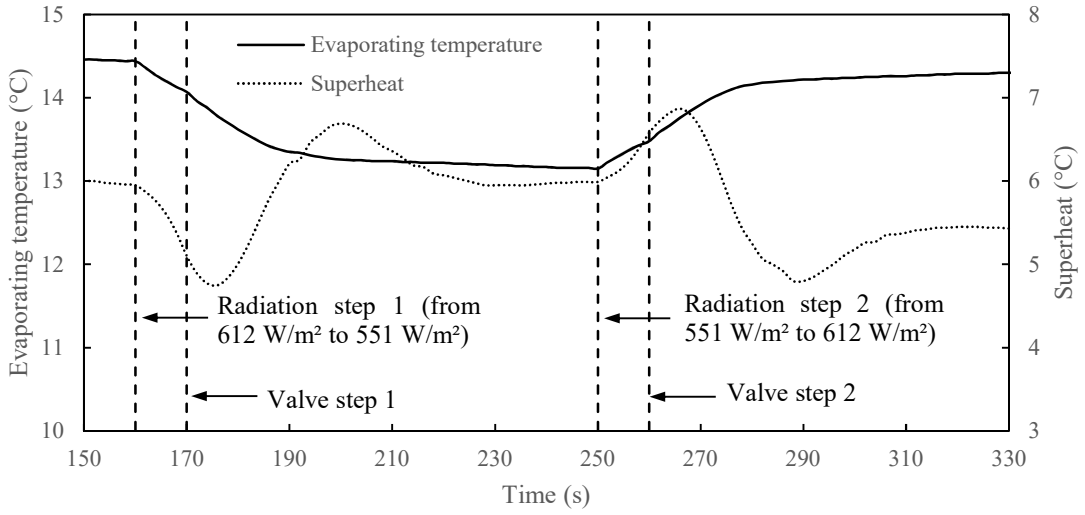

FIGURE 42 - Variation of the superheat and the evaporating temperature.

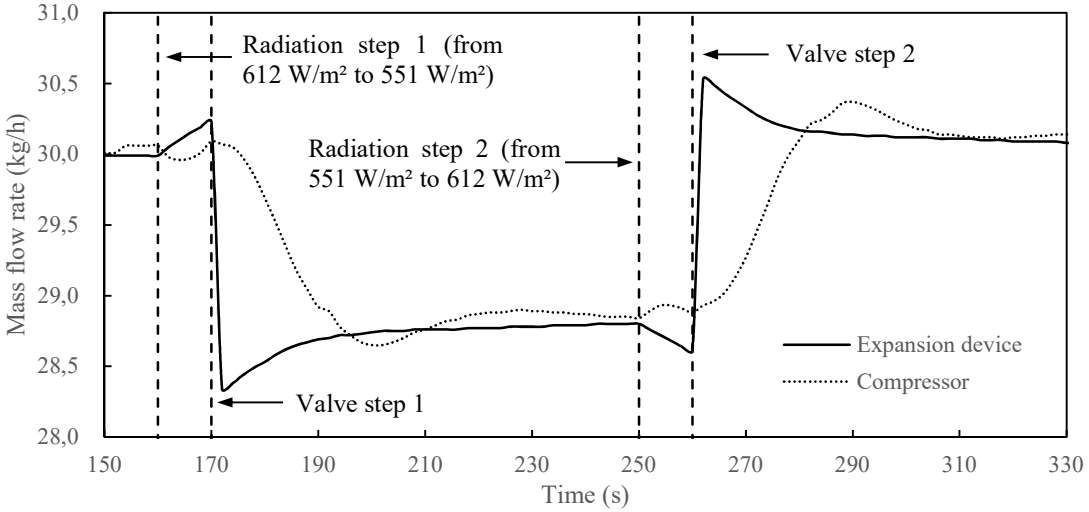

FIGURE 43 - Variation of the mass flow rate in the expansion device and in the compressor.

In order to ensure the compressor integrity, the superheat must be restored to 6°C (set point). Low superheat values may result in the liquid being carried over into the compressor, while high values frequently result in degradation of the lubricant oil, as well as in making it more difficult for the electric motor to properly cool. In order to keep the superheat to its set point, the mass flow rate at the evaporator inlet must be reduced. Thus, at the time of 170 s (Valve step 1), the internal area of the expansion device was reduced by 6.5%. Figure 43 shows this mass flow rate decreasing abruptly to a value a little lower than 28.5 kg/h, but after it increased more slowly until it reached a stable value of 28.8 kg/h. This increase was due to the continuous reduction of evaporating temperature and pressure, which only stabilize after the time of 200 s. It may be noticed that after the abrupt reduction in the mass flow rate of the expansion device, the mass flow

rate imposed by the compressor also decreased, although more slowly. It occurred because the increase in the refrigerant temperature at the compressor inlet, caused by the superheat increase, promoted the decrease of the refrigerant fluid density. It should also be noted that the superheat reached a maximum value of 6.5°C in 200 s, but after that, it decreased and reached the set point around the time of 230 s.

In fact, superheat fluctuations were basically due to the flooding and drying of the evaporator, which was caused by the difference between the refrigerant flows imposed by the expansion device and the compressor. When the first mass flow rate was greater than the other, the evaporator was being flooded, and the superheat decreased. Otherwise, when the compressor mass flow rate was higher, the refrigerant inside the evaporator was drying, so superheat increased. In both cases, the areas between the mass flow rates curves showed in Fig. 43 represent the mass of refrigerant removed from the evaporator or added to it. Note that fluctuations in the mass flow rates and in the superheat did not occur with absolute simultaneity because the temperature response presents greater inertia than the mass flow rate. Therefore, there was always a small delay in the superheat in relation to the mass flow rates. These phenomena can be clearly seen by comparing Figures 42 and 43.

After the system response due to the solar radiation decrease (Radiation Step 1), it reached a new steady state, presenting an evaporating temperature of 13.2°C, a superheat of 6°C and a mass flow rate of 28.8 kg/h. At the time of 250 s, the solar radiation returned to the value of 612 W/m^2 (Radiation step 2), which was the same solar radiation before the Radiation step 1. Then, all processes discussed before occur in the reverse direction. The refrigerant absorbed more energy and its temperature and pressure increased. As a result, the mass flow rate of the expansion device decreased, while the mass flow rate of the compressor hardly varies, so that the superheat increased, as showed in Figures 42 and 43. In order to keep the superheat in the correct value, the internal area of the expansion device was increased by 6.5% at the time of 260 s (Valve step 2), causing the increase of the mass flow rate given by this device. Then, after around 50 s, the evaporating temperature, the superheat and the mass flow rate became 14.3°C, 5.5°C and 30.1 kg/h, respectively. These values were slightly different from the initial values, and this can be attributed to the convergence errors of the model. In particular, superheat was the result of temporal evolutions of temperatures and mass flow rates in the evaporator, so that it is the most sensitive variable to the effects of convergence errors.

Despite these small calculation errors, the most important result of the simulations was that the superheat evolution occurs rapidly and with a small time constant. Changes in solar radiation could happen several times during the day, especially in some seasons. Because of that, the expansion device, to keep the correct value of the superheat, need to act almost immediately and it could operate in a continuous transient condition. Then, an EEV could be more appropriate to control the evaporator superheat of a DX-SAHP. The results presented in Fig. 42 are consistent with the results presented by Sun *et al.* (2014) and Kong *et al.* (Kong; Sun; *et al.*, 2018), when the heat pump is subject to a sudden variation in the solar radiation.

In Fig. 44, CO_2 mass in the evaporator changes because of the mass flow rate variation, due to the change in solar radiation. In the Radiation step 1 (Fig. 43), the mass flow rate through the expansion device increase and the mass flow rate through the compressor remains almost constant. Then, CO_2 mass in the evaporator increase as showed in Fig. 44. On the other hand, in the Radiation step 2 (Fig. 43), the mass flow rate through the expansion device decrease and the mass flow rate through the compressor remains almost constant. As a result, CO_2 mass in the evaporator decrease, as presented in Fig. 44. However, as the valve step occurs only 10 seconds after the Radiation Step, these variations in CO_2 mass are small.

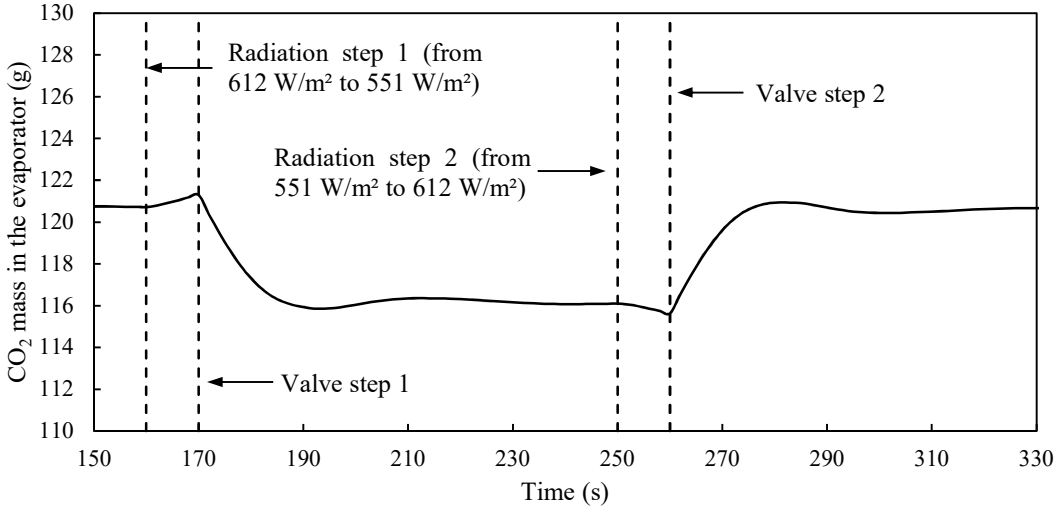

FIGURE 44 - Variation of CO_2 mass in the evaporator.

The more significant variation on the mass flow rate occurs due to valve step. In the valve step 1, as previously discussed, the internal area of the expansion device was reduced. Consequently, the mass flow rate through the expansion device and compressor were also reduced. Although, the mass flow rate through the expansion device becomes smaller than the mass flow rate through the compressor and the evaporator became dryer. The opposite occurs in the valve

step 2. As the valve was opened, the refrigerant floods the evaporator, once the mass flow rate through the expansion device was higher than in the compressor. The decrease and increase of CO_2 mass after Valve Step 1 and 2 are presented in Fig. 44.

The model presented in this work can be a useful tool for determining the EEV control algorithm. The relation between input and output variables can be obtained through curves as those showed in Figures 42 and 43. The model can be used for changing the internal area of the EEV, and then it could provide all data required to obtain the system transfer functions. Furthermore, an adequate control-tuning rule will generate the EEV control algorithm. Finally, it will be possible to use this algorithm in a Programmable Logic Controller or an Embedded System to control the opening of the electronic expansion valve and to keep the superheat in the correct value.

6 CONCLUSIONS

In this thesis, it was carried out the control of a small carbon dioxide direct-expansion solar-assisted heat pump with a low-cost solution using a basic cycle configuration. To provide control is used an embedded system that is an economical alternative. Furthermore, it was analyzed the effect of solar radiation variation on the superheat.

The first part of the conclusions discusses about water heating control. The results showed that the water heating control could affect the optimum high-pressure control. However, it does not affect the superheat control. The system identification and tuning process were appropriate to keep the water outlet temperature at 60°C (to storage) or 45°C (to direct consumption). On the other hand, the variation of CO_2 mass in the DX-SAHP caused oscillations in the water heating control system. The proposed controller was able to keep the correct set point when the expansion valve opening changed, but it was not able to keep the correct set point during the process of the returning oil to the compressor, mainly due to the actuator (water pump) saturation in the minimum value. Finally, the raise of solar radiation resulted in an increase of CO_2 and water mass flow rate and an increase in the COP.

The second part of the conclusions discusses about expansion valve opening. For that purpose, it was considered two different solar radiation conditions, around to 48W/m² and 715 W/m². The ambient temperature, inlet and outlet water temperature are almost the same for both solar radiations. The rise of solar radiation resulted in an increase of 14% in low pressure, 14% in outlet temperature of the compressor, 21% in heat transfer in the gas cooler, 25% in heat transfer in the evaporator, 10% in CO_2 mass flow rate and 21% of the COP. Also, the outlet pressure and temperature in the gas cooler and power consumption of compressor were almost constant.

Moreover, when the expansion valve was opened, the following effects were noticed: compressor discharge pressure decrease, compressor suction pressure increase, outlet temperature of compressor decrease, mass flow rate increase and difference of enthalpy in evaporator and gas cooler decrease. These results are related to the augment in the mass flow rate at the inlet of the evaporator, due to the expansion valve opening. Furthermore, for each solar radiation there is an expansion valve opening that leads the system to the maximum COP. The maximum COP was 2.58 for 715 W/m² and 2.21 for 48 W/m². For HSR and valve opening from 0.15 to 0.30, the COP values are very close, changing from 2.54 to 2.53. For LSR, when considering a valve opening from 0.10 to 0.20, the COP presented similar behavior, changing from 2.17 to 2.13. For the

experimental setup employed in this study, a fixed opening in the expansion device of 0.15-0.20 seems to be suitable for all operating conditions evaluated in this work. The results obtained indicate that, for a small size CO_2 DX-SAHP, using in a basic cycle configuration, a low-cost embedded system water temperature control and a static expansion device as a capillary tube would be suitable for proper control. In this case, the use of a static expansion device can contribute to reducing the system cost without compromise appreciably the system performance.

The third part of the conclusions discusses the effects of the solar radiation variation in the superheat by a distributed mathematical model. It was presented a distributed dynamic model of an evaporator of a direct expansion solar-assisted heat pump. In order to validate the model, a set of experimental tests was performed. The comparison between the experimental results and those obtained with the model show small deviations for the operation of the evaporator in a steady state: 1.5°C for evaporating temperature and 0.2°C for superheating.

The dynamic behavior of the evaporator was evaluated for two situations: when the solar radiation on the evaporator decreases, and when it increases. It was possible to notice the evolution of evaporating temperature, superheat, CO_2 mass flow rate and CO_2 mass in the evaporator. It happens after changes in solar radiation and the internal area of the expansion device.

Simulations using step response have shown that a step variation in solar radiation produced relevant effects in the superheat of the evaporator, indicated that almost immediate action of the expansion device is necessary to correct the superheat to its set point value. Considering the small values for the time constants obtained from the superheat step response and the fact of the system could operate in a continuous transient condition in some seasons, it was concluded that an EEV would be better suited to meet the needs of rapid interventions on the mass flow rate at the evaporator inlet. The data generated using the mathematical model can be useful for determining the transfer functions needed in the development of the EEV control algorithm. Then, in a CO_2 DX-SAHP operating in a dual expansion device configuration the superheat control could be preferable done by an EEV.

REFERENCES

ABNT. *ASSOCIAÇÃO BRASILEIRA DE NORMAS TÉCNICAS. NBR 7198: projeto e execução de instalações prediais de água quente*. . Rio de Janeiro: [s.n.]. , 1993

APREA, Ciro; MAIORINO, Angelo. Heat rejection pressure optimization for a carbon dioxide split system: An experimental study. *Applied Energy*, v. 86, n. 11, p. 2373–2380, 2009.

APREA, Ciro; MASTRULLO, Rita. Experimental evaluation of electronic and thermostatic expansion valves performances using R22 and R407C. *Applied Thermal Engineering*, v. 22, n. 2, p. 205–218, 2002.

ASHRAE. *ASHRAE Guideline 12-2000: Minimizing the risk of legionellosis associated with building water systems*. [S.l: s.n.], 2000.

AUSTIN, Brian T.; SUMATHY, K. *Transcritical carbon dioxide heat pump systems: A review*. *Renewable and Sustainable Energy Reviews*. [S.l: s.n.]. , 2011

BAEK, Changhyun *et al.* Optimal control of the gas-cooler pressure of a CO2heat pump using EEV opening and outdoor fan speed in the cooling mode. *International Journal of Refrigeration*, v. 36, n. 4, p. 1276–1284, 2013.

BENSOUSSAN, Marcos d' Ávilla. *Legionella na Visão de Especialistas*. São Paulo: SETRI Consultoria em Sustentabilidade Ltda, 2014.

CALM, James M. *The next generation of refrigerants - Historical review, considerations, and outlook*. *International Journal of Refrigeration*. [S.l: s.n.]. , 2008

CAMPOS, M.C.M.M., TEIXEIRA, H.C.G. *Controles Típicos de Equipamentos e Processos Industriais*. 2nd editio ed. São Paulo: [s.n.], 2010.

CHATURVEDI, S.; ABAZERI, M. Transient simulation of a capacity-modulated, direct-expansion, solar-assisted heat pump. *Solar Energy*, v. 39 (5), p. 421–428, 1987.

CHATURVEDI, S.; CHEN, D.; KHEIREDDINE, A. Thermal performance of a variable capacity direct expansion solar-assisted heat pump. *Energy Conversion and management*, v. 39 (3), p. 181–191, 1998.

CHEN, Ying; GU, Junjie. The optimum high pressure for CO2 transcritical refrigeration systems with internal heat exchangers. *International Journal of Refrigeration*, v. 28, n. 8, p. 1238–1249, 2005.

CHENG, Lixin *et al.* New flow boiling heat transfer model and flow pattern map for carbon

dioxide evaporating inside horizontal tubes. *International Journal of Heat and Mass Transfer*, 2006.

CHENG, Lixin *et al.* New prediction methods for CO2evaporation inside tubes: Part I - A two-phase flow pattern map and a flow pattern based phenomenological model for two-phase flow frictional pressure drops. *International Journal of Heat and Mass Transfer*, 2008.

CHUA, K. J.; CHOU, S. K.; YANG, W. M. *Advances in heat pump systems: A review*. *Applied Energy*. [S.l: s.n.]. , 2010

DUARTE, WILLIAN MOREIRA. *NUMERIC MODEL OF A DIRECT EXPANSION SOLAR ASSISTED HEAT PUMP WATER HEATER OPERATING WITH LOW GWP REFRIGERANTS (R1234YF, R290, R600A AND R744) FOR REPLACEMENT OF R134A. PhD thesis.* 2018. 109 f. 2018.

DUFFIE, John A.; BECKMAN, William A. *Solar Engineering of Thermal Processes: Fourth Edition*. [S.l: s.n.], 2013.

EPE. Balanço Energético nacional 2017: Ano base 2016, Relatório Síntese. *Empresa de Pesquisa Energética - Rio de janeiro: EPE, 2017*, p. 292, 2017.

FAIRES, V.M.; SIMMANG, C.M. *Termodinâmica*. 6th editio ed. Rio de Janeiro: [s.n.], 1983.

FARIA, Ralney N. *et al.* Dynamic modeling study for a solar evaporator with expansion valve assembly of a transcritical CO2 heat pump. *International Journal of Refrigeration*, v. 64, p. 203–213, 2016.

FARIA, Ralney Nogueira. *Projeto e construção de uma bomba de calor a CO2 operando em ciclo transcrítico e modelagem dinâmica do conjunto evaporador solar-válvula de expansão. Ph.D Thesis. UFMG.* 2013.

FONSECA, Euler Assunção Costa. *Projeto de um controlador para o ajuste da temperatura de água de uma bomba de calor com evaporador solar. Under graduate course work. UFMG*. 2018.

GE, Y. T.; TASSOU, S. A. Control optimizations for heat recovery from CO2 refrigeration systems in supermarket. *Energy Conversion and Management*, v. 78, p. 245–252, 2014.

GECR. *Kyoto Protocol to the United Nations Framework Conservation on Climate Change. Global Environmental Change Report, New York, USA.* . New York, NY, USA,: [s.n.], 1997.

GRANRYD, Eric. *Refrigerating Engineering - Part II*. Department ed. Stockholm: [s.n.], 2005.

GROLL, Eckhard; KIM, Jun-Hyeung. Review Article: Review of Recent Advances toward

Transcritical CO2 Cycle Technology. *HVAC&R Research*, v. 13, n. 3, p. 499–520, 2007.

HEPBASLI, Arif; KALINCI, Yildiz. *A review of heat pump water heating systems*. *Renewable and Sustainable Energy Reviews*. [S.l: s.n.]. , 2009

HOU, Yu; MA, Juanli; *et al.* Experimental investigation on the influence of EEV opening on the performance of transcritical CO2refrigeration system. *Applied Thermal Engineering*, v. 65, n. 1–2, p. 51–56, 2014.

HOU, Yu; LIU, Changhai; *et al.* Mass flowrate characteristics of supercritical CO2flowing through an electronic expansion valve. *International Journal of Refrigeration*, 2014.

HU, Bin *et al.* Extremum seeking control of COP optimization for air-source transcritical CO2 heat pump water heater system. *Applied Energy*, v. 147, p. 361–372, 2015.

HUHTINIEMI, Ilpo K.; CORRADINI, Michael L. Condensation in the presence of noncondensable gases. *Nuclear Engineering and Design*, 1993.

INCROPERA, Frank P.; DEWITT, David P. *Fundamentos de Transferencia de Calor*. [S.l: s.n.], 1999.

ISLAM, M. R. *et al.* Performance study on solar assisted heat pump water heater using CO2 in a transcritical cycle. 2012, [S.l: s.n.], 2012.

ITO, S.; MIURA, N.; WANG, K. Performance of a heat pump using direct expansion solar collectors. *Solar Energy*, v. 65, n. 3, p. 189–196, 1999.

JOINT COMMITTEE FOR GUIDES IN METROLOGY. *Evaluation of measurement data — Guide to the expression of uncertainty in measurement*. *Joint Committee for Guides in Metrology*. [S.l: s.n.], 2008.

KALOGIROU, S.A. *Solar Energy Engineering: Processes and Systems*. [S.l: s.n.], 2009.

KARA, Ozer; ULGEN, Koray; HEPBASLI, Arif. *Exergetic assessment of direct-expansion solar-assisted heat pump systems: Review and modeling*. *Renewable and Sustainable Energy Reviews*. [S.l: s.n.]. , 2008

KIM, B. R. *et al. Literature review - Efficacy of various disinfectants against Legionella in water systems*. *Water Research*. [S.l: s.n.]. , 2002

KIM, M.S.; SHIN, C.S.; KIM, M.S. A study on the real time optimal control method for heat rejection pressure of a CO2 refrigeration system with an internal heat exchanger. *International Journal of Refrigeration*, v. 48, 2014.

KONG, X. Q. *et al.* Modeling evaluation of a direct-expansion solar- assisted heat pump water

heater using R410A. *International Journal of Refrigeration*, v. 76, p. 136–146, 2017.
KONG, X.Q. *et al.* Thermal performance analysis of a direct-expansion solar-assisted heat pump water heater. *Energy*, v. 36, n. 12, p. 6830–6838, 2011.
KONG, Xiangqiang; JIANG, Kailin; *et al.* Control strategy and experimental analysis of a direct-expansion solar-assisted heat pump water heater with R134a. *Energy*, v. 145, p. 17–24, 2018.
KONG, Xiangqiang; SUN, Penglong; *et al.* Experimental performance analysis of a direct-expansion solar-assisted heat pump water heater with R134a in summer. *International Journal of Refrigeration*, v. 91, p. 12–19, 2018.
LI, Y. *et al.* Experimental performance analysis on a direct-expansion solar-assisted heat pump water heater. *Applied Thermal Engineering*, v. 27 (17), p. 2858–2868, 2007.
LIAO, S. M.; ZHAO, T. S.; JAKOBSEN, A. Correlation of optimal heat rejection pressures in transcritical carbon dioxide cycles. *Applied Thermal Engineering*, v. 20, n. 9, p. 831–841, 2000.
LIU, Changhai *et al.* Experimental study on the CO2 flow characteristics through electronic expansion valves in heat pump. *International Journal of Refrigeration*, 2016.
LIU, Cichong *et al.* Mass flow characteristics and empirical modeling of R744 flow through electronic expansion device. *International Journal of Refrigeration*, 2018.
LORENTZEN, Gustav. Revival of carbon dioxide as a refrigerant. *International Journal of Refrigeration*, v. 17, n. 5, p. 292–301, 1994.
LORENTZEN, Gustav. Transcritical vapour compression cycle device. *Patent WO/07683*, 1990.
MA, Yitai; LIU, Zhongyan; TIAN, Hua. *A review of transcritical carbon dioxide heat pump and refrigeration cycles*. *Energy*. [S.l: s.n.]. , 2013
MINETTO, Silvia. Theoretical and experimental analysis of a CO2 heat pump for domestic hot water. *International Journal of Refrigeration*, v. 34, n. 3, p. 742–751, 2011.
MOHAMED, Elamin; RIFFAT, Saffa; OMER, Siddig. Low-temperature solar-plate-assisted heat pump: A developed design for domestic applications in cold climate. *International Journal of Refrigeration*, v. 81, p. 134–150, 2017.
MOHANRAJ, M.; JAYARAJ, S.; MURALEEDHARAN, C. *Environment friendly alternatives to halogenated refrigerants-A review*. *International Journal of Greenhouse Gas Control*. [S.l: s.n.]. , 2009
MOLINA, Mario J.; ROWLAND, F. S. Stratospheric sink for chlorofluoromethanes: Chlorine atomc-atalysed destruction of ozone. *Nature*, v. 249, n. 5460, p. 810–812, 1974.

MORENO-RODRIGUEZ, A. *et al.* Experimental validation of a theoretical model for a direct-expansion solar-assisted heat pump applied to heating. *Energy*, v. 60, p. 242–253, 2013.

OLIVEIRA, R. N. *Modelo dinâmico e estudo experimental para um resfriador de uma bomba de calor operando com CO2 para aquecimento de água residencial. Ph.D Thesis. UFMG.* 2013.

OMOJARO, Peter; BREITKOPF, Cornelia. *Direct expansion solar assisted heat pumps: A review of applications and recent research*. *Renewable and Sustainable Energy Reviews*. [S.l: s.n.]. , 2013

OZISIK, M.N. *Heat Transfer, a Basic Approach*. New York: [s.n.], 1985.

PALYVOS, J. A. *A survey of wind convection coefficient correlations for building envelope energy systems' modeling*. *Applied Thermal Engineering*. [S.l: s.n.]. , 2008

PARK, Chasik *et al.* Mass flow characteristics and empirical modeling of R22 and R410A flowing through electronic expansion valves. *International Journal of Refrigeration*, 2007.

PEARSON, Andy. Carbon dioxide—new uses for an old refrigerant. *International Journal of Refrigeration*, v. 28, n. 8, p. 1140–1148, 2005.

PEÑARROCHA, Ignacio *et al.* A new approach to optimize the energy efficiency of CO2 transcritical refrigeration plants. *Applied Thermal Engineering*, v. 67, n. 1–2, p. 137–146, 2014.

PÉREZ-GARCÍA, V. *et al.* Comparative study of transcritical vapor compression configurations using CO2as refrigeration mode base on simulation. *Applied Thermal Engineering*, 2013.

QI, Peng Cheng *et al.* Experimental investigation of the optimal heat rejection pressure for a transcritical CO2 heat pump water heater. *Applied Thermal Engineering*, v. 56, n. 1–2, p. 120–125, 2013.

ROUHANI, S. Z.; AXELSSON, E. Calculation of void volume fraction in the subcooled and quality boiling regions. *International Journal of Heat and Mass Transfer*, 1970.

SALAZAR, M.; MÉNDEZ, F. PID control for a single-stage transcritical CO2 refrigeration cycle. *Applied Thermal Engineering*, v. 67, n. 1–2, p. 429–438, 2014.

SARBU, Ioan. *A review on substitution strategy of non-ecological refrigerants from vapour compression-based refrigeration, air-conditioning and heat pump systems*. *International Journal of Refrigeration*. [S.l: s.n.]. , 2014

SARKAR, J.; BHATTACHARYYA, Souvik; GOPAL, M. Ram. Simulation of a transcritical CO2heat pump cycle for simultaneous cooling and heating applications. *International Journal of Refrigeration*, v. 29, n. 5, p. 735–743, 2006.

SARKAR, J.; BHATTACHARYYA, Souvik; GOPAL, M.Ram. Optimization of a transcritical CO2 heat pump cycle for simultaneous cooling and heating applications. *International Journal of Refrigeration*, v. 27, n. 8, p. 830–838, 2004.

SHAO, Shuangquan *et al.* A new inverter heat pump operated all year round with domestic hot water. *Energy Conversion and Management*, v. 45, n. 13–14, p. 2255–2268, 2004.

SUN, Xiaolin *et al.* Experimental study on roll-bond collector/evaporator with optimized-channel used in direct expansion solar assisted heat pump water heating system. *Applied Thermal Engineering*, v. 66, n. 1–2, p. 571–579, 2014.

SUN, Xiaolin *et al.* Performance Comparison of Direct Expansion Solar-assisted Heat Pump and Conventional Air Source Heat Pump for Domestic Hot Water. 2015, [S.l: s.n.], 2015.

UNEP. *Montreal Protocol on Substances that Deplete the Ozone Layer. United Nations Environment Program, New York, USA.* . New York, NY, USA: [s.n.], 1987.

VASCONCELLOS, L. E. M.; LIMBERGER, M. A. C. (Organizadores). *Energia Solar para aquecimento de água no Brasil: Contribuições da Eletrobrás Procel e Parceiros.* Rio de Janeiro: [s.n.], 2012.

WANG, Shouguo *et al.* Experimental investigation on air-source transcritical CO2heat pump water heater system at a fixed water inlet temperature. *International Journal of Refrigeration*, v. 36, n. 3, p. 701–716, 2013.

WILLEM, H.; LIN, Y.; LEKOV, A. *Review of energy efficiency and system performance of residential heat pump water heaters*. *Energy and Buildings*. [S.l: s.n.]. , 2017

XU, Guoying; ZHANG, Xiaosong; DENG, Shiming. A simulation study on the operating performance of a solar-air source heat pump water heater. *Applied Thermal Engineering*, v. 26, n. 11–12, p. 1257–1265, 2006.

YANG, Liang *et al.* Minimizing COP loss from optimal high pressure correlation for transcritical CO<inf>2</inf> cycle. *Applied Thermal Engineering*, v. 89, p. 656–662, 2015.

ZHANG, Jian-Fei; QIN, Yan; WANG, Chi-Chuan. Review on CO2 heat pump water heater for residential use in Japan. *Renewable and Sustainable Energy Reviews*, v. 50, p. 1383–1391, 2015.

ZHANG, X. P. *et al.* Theoretical and experimental studies on optimum heat rejection pressure for a CO2 heat pump system. *Applied Thermal Engineering*, v. 30, n. 16, p. 2537–2544, 2010.

APPENDIX A - Papers

This PhD thesis is the result of research conducted at the group of refrigeration and heating (GREA) at Universidade Federal de Minas Gerais (UFMG) under the supervision of Prof. Antônio Maia and Prof. Luiz Machado and at the division of Applied Thermodynamics at Royal Institute of Technology (KTH), under the supervision of Prof. Björn Palm. During this time, four journal papers and eight conference/congress papers related to this research were produced and they are listed below:

1. **PAULINO, T. F.**; OLIVEIRA, R. N.; MAIA, A. A. T.; PALM, B.; MACHADO, L. Modeling and experimental analysis of the solar radiation in a CO_2 direct-expansion solar-assisted heat pump. *Applied Thermal Engineering*, v. 148, p. 160-172, 2019.

2. RABELO, S. N.; **PAULINO, T. F.**; DUARTE, W. M.; MAIA, A. A. T., MACHADO, L. Experimental analysis of the influence of the expansion valve opening on the performance of the small size CO_2 solar assisted heat pump. *Submitted to Applied Thermal Engineering*. *Under review.*

3. **PAULINO, T. F.**; FONSECA, E. A. C.; MAIA, A. A. T.; MACHADO, L.; KOURY, R. N. N. Design of an embedded system for water temperature control in a solar assisted heat pump. In: International Congress of Mechanical Engineering - 24th COBEM. Curitiba - PR. ABCM, 2017.

4. **PAULINO, T. F.**; OLIVEIRA, R. N.; MACHADO, L.; KOURY, R. N. N. Effects of solar radiation in a direct expansion solar assisted CO_2 heat pump. In: International Congress of Mechanical Engineering - 24th COBEM. Curitiba - PR. ABCM, 2017.

5. **PAULINO, T. F.**; OLIVEIRA, R. N.; MACHADO, L.; KOURY, R. N. N. Distributed model to achieve the steady state through the false transient in a solar assisted heat pump. In: International Congress of Mechanical Engineering - 24th COBEM. Curitiba - PR. ABCM, 2017.

6. RABELO, S. N.; **PAULINO, T. F.**; DUARTE, W. M.; SAWALHA, S.; MACHADO, L. Experimental Analysis of the Influence of Water Mass Flow Rate on the Performance of a CO_2 Direct-Expansion Solar Assisted Heat Pump. 20th International Conference on Energy, Environmental and Chemical Engineering. Stockholm. v.7, p.556 - 560, 2018.

7. DUARTE, W. M.; **PAULINO, T. F.**; RABELO, S. N.; MAIA, A. A. T.; MACHADO, L. Optimal high pressure correlation for R744 direct expansion solar assisted heat pump for domestic hot water. In: 17TH Brazilian Congress of Thermal Sciences and Engineering - ENCIT. Águas de Lindóia-SP: ABCM, 2018.

8. RABELO, S. N.; DUARTE, W. M.; **PAULINO, T. F.**; GARCIA, J.; MACHADO, L. Analysis of the refrigerant mass charge for a direct expansion solar assisted heat pump system. In: 17TH

Brazilian Congress of Thermal Sciences and Engineering - ENCIT. Águas de Lindóia-SP: ABCM, 2018.

9. DUARTE, W. M.; DINIZ, H. A. G.; **PAULINO, T. F.**; RABELO, S. N.; MACHADO, L. Performance comparison of direct expansion solar assisted heat pump working with R1234yf as a drop-in replacement for R134a. In: 17TH Brazilian Congress of Thermal Sciences and Engineering - ENCIT. Águas de Lindóia-SP: ABCM, 2018.

10. DUARTE, W. M.; RABELO, S. N.; **PAULINO, T. F.**; PALM, B.; MACHADO, L. Economic and energetic analysis of solar collector size of a direct expansion solar assisted heat pump In: 17TH Brazilian Congress of Thermal Sciences and Engineering - ENCIT. Águas de Lindóia-SP: ABCM, 2018.

11. DUARTE, W. M.; **PAULINO, T. F.**; GARCIA, J.; SAWALHA, S.; MACHADO, L.; Refrigerants selection for a direct expansion solar assisted heat pump for domestic hot water. *Solar Energy*, v. 184, p. 527-538, 2019.

12. RABELO, S. N.; **PAULINO, T. F.**; SOARES, C. P. M.; MACHADO, L; OLIVEIRA, R. N. Mass flow characteristics of CO_2 operating in a transcritical cycle flowing through a needle expansion valve in a direct-expansion solar assisted heat pump. *Submitted to Applied Thermal Engineering. Under review.*

From papers 1 to 3 are presented the main thesis results. The paper number 1 presents the results related to the evaluation of the effects of the solar radiation variation in the superheat. The paper number 2 shows the results related to evaluation of the expansion valve opening. The pumper number 3 presents part of the results related to the water heating control system. From papers 1 to 12, the author of this thesis was responsible for experimental tests or part of them and assisted in the writing and result analysis. The paper number 6 was chosen as the best paper of the 20th International Conference on Energy, Environmental and Chemical Engineering.

APPENDIX B - C program language for the control water heating system

```
#include<16F877A.h>
#device ADC=10
#use delay(clock=4000000)
#fuses HS, NOWDT, PUT, NOPROTECT, NODEBUG, NOBROWNOUT, NOLVP
#use rs232(BAUD=1200,XMIT=PIN_C6,RCV=PIN_C7,PARITY=N,BITS=8)
#include <lcd2.c>
#include <stdlib.h>
#define ONE_WIRE_PIN PIN_D0

int ciclos=0;
int led=0;
signed int16 duty=0;
int32 segundos = 0;

// PID
long int dss=0;
float somaI=0, erro=0, erro0=0, integral, proporcional;
float dt; //Ajustar
float derivativo, PV=0;
//variáveis pid
float kp=4.37, ki=0.18, kd=6.51, saida=100;
float SP=60.0;

float temperature=-1;

//////////PID//////////
void PID()
{
  dt = dss;
  PV=temperature;
  erro= PV - SP;

  if((saida<100)&&(saida>0))
  {
    //Integral part
    somaI=somaI+((erro+erro0)/2);//*dt/1000.0;//Check time
    integral=ki*somaI;
    if (integral>=100) integral=100;
    if (integral<=-100) integral=-100;
```

```
  }

  //Proportional part
  proporcional=kp*erro;

  //Derivative part
  derivativo=kd*(erro-erro0);//*(1000.0/dt);//Conferir base de tempo

  //Controller outlet
  saida=proporcional+integral+derivativo;
  if (saida<=-100) saida=-100;
  if (saida>=100) saida=100;

  dss=0;
  erro0=erro;

}
//////////PID//////////
//////// TEMPERATURE SENSOR ///////////////////////
void onewire_reset()  // OK if just using a single permanently connected device
{
  output_low(ONE_WIRE_PIN);
  delay_us( 500 ); // pull 1-wire low for reset pulse
  output_float(ONE_WIRE_PIN); // float 1-wire high
  delay_us( 500 ); // wait-out remaining initialisation window.
  output_float(ONE_WIRE_PIN);
}

void onewire_write(int data)
{
 int count;

 for (count=0; count<8; ++count)
 {
  output_low(ONE_WIRE_PIN);
  delay_us( 2 ); // pull 1-wire low to initiate write time-slot.
  output_bit(ONE_WIRE_PIN, shift_right(&data,1,0)); // set output bit on 1-wire
  delay_us( 60 ); // wait until end of write slot.
  output_float(ONE_WIRE_PIN); // set 1-wire high again,
  delay_us( 2 ); // for more than 1us minimum.
 }
```

```
}

int onewire_read()
{
 int count, data;

 for (count=0; count<8; ++count)
 {
  output_low(ONE_WIRE_PIN);
  delay_us( 2 ); // pull 1-wire low to initiate read time-slot.
  output_float(ONE_WIRE_PIN); // now let 1-wire float high,
  delay_us( 8 ); // let device state stabilise,
  shift_right(&data,1,input(ONE_WIRE_PIN)); // and load result.
  delay_us( 120 ); // wait until end of read slot.
 }

 return( data );
}

float ds1820_read()
{
  int8 busy=0, temp1, temp2;
  signed int16 temp3;
  float result;

  onewire_reset();
  onewire_write(0xCC);
  onewire_write(0x44);

  while (busy == 0)
  busy = onewire_read();
  onewire_reset();
  onewire_write(0xCC);
  onewire_write(0xBE);
  temp1 = onewire_read();
  temp2 = onewire_read();
  temp3 = make16(temp2, temp1);

 result = (float) temp3 / 16.0;  //Calculation for DS18B20 with 0.1 deg C resolution
 return(result);
}
```

```
//////// TEMPERATURE SENSOR //////////////////////

int temp0 = 0;
int temp1 = 1;

#int_timer0
void tempo(){
  ciclos++;
  if (ciclos==125){
    //led =(!led);
    segundos += 1;
    temp0=(!temp0);
    ciclos=0;
  }
  set_timer0(6-get_timer0());
}

void main (void)
{
  lcd_init();
  setup_timer_0(RTCC_INTERNAL|RTCC_DIV_32);
  enable_interrupts(global|int_timer0);
  set_timer0(6);
  setup_timer_2(T2_DIV_BY_4,255,1);
  setup_ccp2(ccp_pwm);
  duty = 450;
  while(true){
    if(segundos<=30){
      if(temp0!=temp1){
        duty = 400;
        temp0=temp1;
        set_pwm2_duty(duty);
        temperature = ds1820_read();
        while(temperature==-1){
          delay_ms(100);
        }
        lcd_gotoxy(1,1);
        printf(lcd_putc,"\fT:%3.1f %ld", temperature,duty);
        lcd_gotoxy(1,2);
        printf(lcd_putc,"t:%ld",segundos);
        printf("%.2f %ld %ld*\n\r",temperature,duty,segundos);
```

```
      }
    }
    //where bottom is pressed the LED status changed
//!    if(input(PIN_B0)==0){
//!      delay_ms(100);
//!      if(input(PIN_B0)==0){
//!        duty += 30;
//!        //led_botao=!led_botao;
//!      }
//!    }
//!    if(led_botao)
//!      output_high(PIN_B5);
//!     else
//!      output_low(PIN_B5);
//!
    else{
      if(temp0!=temp1){
        temp0=temp1;
        temperature = ds1820_read();
        while(temperature==-1){
          delay_ms(100);
        }
        PID();
        duty = (1023.0 - 300)*(saida/100) +300;

        if (duty>1023) duty = 1023;
        if (duty<300) duty = 300;

        set_pwm2_duty(duty); // Define Duty cycle.

        lcd_gotoxy(1,1);
        printf(lcd_putc,"\fT:%3.1f %ld", temperature,duty);
        lcd_gotoxy(1,2);
        printf(lcd_putc,"t:%ld",segundos);

         printf("T:%.2f PWM:%ld t:%ld*\n\r",temperature,duty,segundos);
      }
    }
  }
}
```

APPENDIX C - Development of model equations

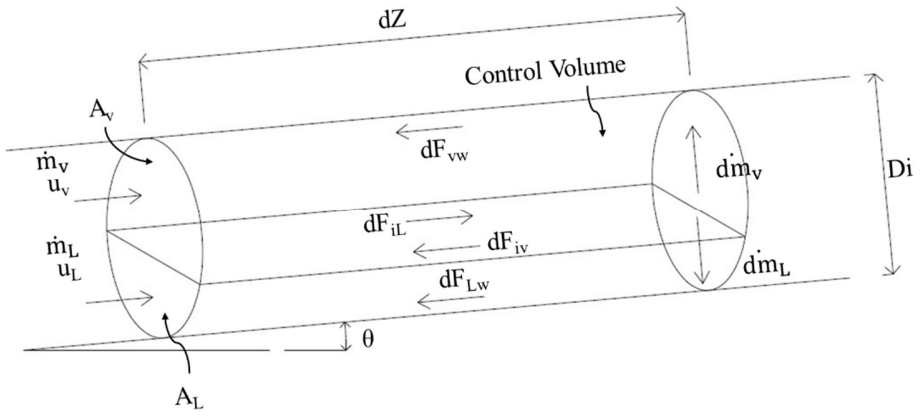

Figure C.1: Control volume for a two-phase flow in a tube.

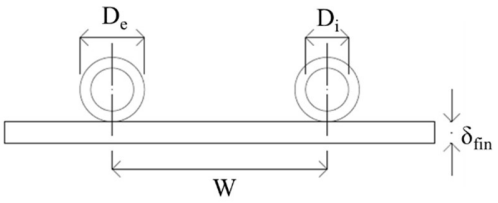

Figure C.2: Plate and tube dimensions - Evaporator/Collector.

Mass balance – Continuity Equation

The rate of change of mass within the control volume showed in Figure C.1 is given by Equations C.1 and C.2.

$$\frac{\partial m}{\partial t} = \frac{\partial(\rho.A.dz)}{\partial t} = A.dz.\frac{\partial \rho}{\partial t} \tag{C.1}$$

$$\frac{\partial m}{\partial t} = -\frac{\partial \dot{m}}{\partial z}.dz = -\frac{\partial(G.A)}{\partial z}.dz = -A.dz.\frac{\partial G}{\partial z} \tag{C.2}$$

Then, by combining Equations C.1 and C.2, Equation C.3 (Eq. 15) is obtained:

$$\frac{\partial G_f}{\partial z} = -\frac{\partial \rho_f}{\partial t} \tag{C.3 (Eq. 15)}$$

Energy balance - First Law of Thermodynamics

The First Law of Thermodynamics applied to the control volume showed in Figure C.1 is given by Equation C.4:

$$\frac{\partial}{\partial t}\left[\rho_f.A.dz\left(h_f - P_f.v_f\right)\right] = H_f.p_f.dz.\left(T_w - T_f\right) - 0 - \Delta\left(G_f.A.h_f\right) \tag{C.4}$$

Taking Equation C.4, divided by dz and the derivate of the first and of the last term, Equation C.5 is obtained:

$$A\left(\frac{\partial \rho_f}{\partial t}h_f + \frac{\partial h_f}{\partial t}\rho_f - \frac{\partial P_f}{\partial t}\right) = H_f.p_f\left(T_w - T_f\right) - A\left(\frac{\partial G_f}{\partial z}h_f + \frac{\partial h_f}{\partial z}G_f\right) \quad \text{(C.5)}$$

By combining Equations C.3 and C.5, Equation C.6 is obtained. By isolating the enthalpy gradient, Equation C.7 is achieved:

$$A\left(\frac{\partial h_f}{\partial t}\rho_f - \frac{\partial P_f}{\partial t}\right) = -A\frac{\partial h_f}{\partial z}G_f + H_f p_f\left(T_w - T_f\right) \quad \text{(C.6)}$$

$$\frac{\partial h_f}{\partial z} = \frac{1}{G_f}\left[\frac{\partial P_f}{\partial t} - \rho_f\frac{\partial h_f}{\partial t} + H_f\frac{p_f}{A_f}\left(T_w - T_f\right)\right] \quad \text{(C.7) (Eq. 14)}$$

Momentum balance - Reynolds Transport Theorem

Appling the momentum balance in the vapor phase:

$$-A_v\frac{\partial P_f}{\partial z}dz - dF_{vw} - dF_{iv} - A_v\rho_v dz.g.\sin(\theta) = \frac{\partial\left(\dot{m}_v dz\right)}{\partial t} + \frac{\partial}{\partial z}\left(\dot{m}_v u_v\right)dz + -d\dot{m}_v u_L \quad \text{(C.8)}$$

Appling the momentum balance in the liquid phase:

$$-A_L\frac{\partial P}{\partial z}dz - dF_{Lw} - dF_{iL} - A_L\rho_L dz.g.\sin(\theta) = \frac{\partial\left(\dot{m}_L dz\right)}{\partial t} + \frac{\partial}{\partial z}\left(\dot{m}_L u_L\right)dz + -d\dot{m}_L u_L \quad \text{(C.9)}$$

Through the balance of forces in the interfaces:

$$dF_{iL} = dF_{iv}; d\dot{m}_v = -d\dot{m}_L$$

Adding Equations C.8 and C.9:

$$-A\frac{\partial P}{\partial z}dz - dF_{vw} - dF_{Lw} - dz.g.\sin(\theta)\left(A_v\rho_v + A_L\rho_L\right) = \frac{\partial}{\partial t}\left(\dot{m}_v + \dot{m}_L\right)dz + + \frac{\partial}{\partial z}\left(\dot{m}_v u_v + \dot{m}_L u_L\right)dz \quad \text{(C.10)}$$

Considering the follow equations and replacing it in Equation C.10, Equation C.11 is obtained:

$$x = \frac{\dot{m}_v}{\dot{m}_v + \dot{m}_L}; u_v = \frac{\dot{m}_v}{\rho_v A_v}; u_L = \frac{\dot{m}_L}{\rho_L A_L}; \alpha = \frac{A_v}{A_v + A_L}; -\left(\frac{dP}{dz}\right)_{fr} = \frac{dF_{vw}}{Adz} + \frac{dF_{Lw}}{Adz}$$

$$\frac{\partial}{\partial z}\left\{P_f + G_f^2\left[\frac{x^2 v_v}{\alpha} + \frac{(1-x)^2 v_l}{1-\alpha}\right]\right\} = -\frac{\partial G}{\partial t} - \left(\frac{dP}{dz}\right)_{fr} + -g\sin(\theta)\left[\alpha\rho_v + (1-\alpha)\rho_L\right] \quad \text{(C.11)}$$

Calling the term between braces as modified pressure ($\overline{P_f}$), represented by Equation C.12 (Eq. 16B), Equation C.13 (Eq. 16A) is obtained:

$$\overline{P_f} = P_f + G_f^2 \left[\frac{x^2 v_v}{\alpha} + \frac{(1-x)^2 v_l}{1-\alpha} \right] \qquad \text{(C.12) (Eq. 16B)}$$

$$\frac{d\overline{P_f}}{dz} = -\frac{\partial G_f}{\partial t} - \left(\frac{dP}{dz} \right)_{fr} - g\rho_f \sin(\theta) \qquad \text{(C.13) (Eq. 16A)}$$

Balance of energy applied for the coil - First Law of Thermodynamics

The First Law of Thermodynamics applied to the coil showed in Figure C.2 is given by Equation C.14 (Eq.17). The first term in the right side of Equation C.14 is presented in Duffie and Beckman (2006):

$$\rho_w A_w c_{pw} \frac{\partial T_w}{\partial t} = \left[(W - D_0) F + D_0 \right] \left[S - U_L \left(T_w - T_{sky} \right) \right] + \\ - H_f A_f \left(\mathrm{T_w} - \mathrm{T_f} \right) \qquad \text{(C.14)(Eq. 17)}$$